Villar I Comajoan, Laia

Dr. Joan Llorens Llacuna
Departament d'Enginyeria Química I Química Analítica

Grau en Enginyeria Química

Treball Final de Grau

Use of CFD code to calculate heat transfer coefficients in pipes with extended surface and turbulent promoters

Laia Villar i Comajoan

June 2019

UNIVERSITAT DE BARCELONA

CONTENTS

SUMMARY

In this project, heat transfer and pressure drop performance of pipes with extended surface and different twisted tape inserts were simulated with ANSYS Fluent © software. The studied pipes were characterized by height and length of the surface crests and the twist of the twisted tape insert.

After a superficial exploration of meshes and turbulence models for a single pipe, k-ω SST model was chosen to make further. The results obtained with CFD were compared with experimental data to confirm the veracity of the simulations, which show a higher exactitude for temperature outlet compared to pressure drop.

After that, it was seen how the geometric characteristics affect to heat transfer and pressure drop. Both heat transfer and pressure drop increase when the insert curvature and the crests size increase, in other words, when turbulence is promoted.

Finally, the Thermal Performance Factor was calculated to see if the heat transfer enhancement was worth the pressure drop increase. The TPF showed a result >1, confirming that the performance of the modified pipes is better than a plain cylindrical pipe.

Keywords: CFD, heat transfer, thermal performance factor, extended surface, turbulent promoters

RESUM

En aquest treball s'ha simulat el comportament pel que fa a l'intercanvi de calor i la pèrdua de càrrega de tubs amb la superfície estesa i una cinta retorçada dins. Totes les simulacions s'han realitzat amb el programari d'ANSYS Fluent ©. Els tubs estudiats es caracteritzen per l'altura i llargada de les crestes de la superfície i la curvatura de la cinta.

Per tal d'optimitzar la simulació s'ha realitzat una exploració superficial de mallats i models de turbulència, i el model escollit ha estat k-ω SST. Per tal de comprovar la veracitat dels resultats obtinguts s'han comparat amb resultats experimentals dels mateixos experiments. S'ha vist que les temperatures de sortida són més similars a les experimentals que les pèrdues de càrrega.

Seguidament s'ha vist com les característiques dels tubs afecten a la transferència de calor i la pèrdua de càrrega. Les dues propietats augmenten amb la mida de les crestes i la curvatura de les cintes, és a dir, quan augmenta la turbulència.

Finalment, a partir del factor de rendiment tèrmic, s'ha vist que el comportament dels tubs modificats és millor que el d'un tub cilíndric simple. Que la majoria d'experiments presentin valors superiors a la unitat vol dir que l'augment en la transferència de calor és més important que la pèrdua de càrrega.

Paraules clau: CFD, bescanvi de calor, factor de rendiment tèrmic, superfície estesa, promotors de turbulència.

1. INTRODUCTION

Shell and tube heat exchangers are widely used, not only in chemical industry but also in food and energy industries and vehicles. The amount of heat exchanged is a function of the heat transfer surface and the fluid convection, therefore the fluid turbulence. In order to maximize heat exchange, modifications are made to the tube. By adding roughness or fins to the tube and using different pipe geometries the heat exchange surface can be increased. To increase turbulence, swirl producing devices as twisted or wavy tapes and wire coil inserts can be used, as well as perforating this inserts.

All the mentioned modifications, while they augment the heat exchange, they also produce higher pressure drops than a simple cylindrical tube. The reason to apply modifications to the tubes is to improve the whole process performance, as a consequence it is important to take pressure drop into account. It could be that the increase in heat exchange is not worth the increase in power consumption due to pumping ability to maintain the fluid flow.

1.1. HEAT TRANSFER

Exchange of thermal energy in the form of heat can be classified into three mechanisms: conduction, convection and radiation.

Molecular conduction of heat is the transfer mechanism typical in solid materials, and it is exclusive of those and fluids at rest. When there is a temperature gradient in a physical environment, heat flows from in the opposite direction of the gradient. Energy is transferred due to the movement and collisions of particles forming the matter, such as atoms, molecules, ions or electrons. Fourier's law (1.1) connects the heat flow through a unit area with the temperature gradient with a proportional constant called thermal conductivity.

$$\vec{q} = -k\,\nabla T \tag{1.1}$$

Thermal conductivity is characteristic of each material and can be affected by its physical state and by temperature.

Heat transfer in convection mechanism takes place because of the movement of the matter in the system. It is the most important mechanism in fluid systems because even when the fluid is at rest, temperature gradients create density differences, which generate buoyancy forces, leading to the fluid circulation. Natural and artificial convection can be differentiated. Natural convection is caused by the buoyancy forces the density differences cause. In the case of artificial convection, the fluid is moved by mechanical devices such as pumps, fans or mixers.

In order to evaluate the convective heat transfer, microscopic momentum, energy and mass balances should be solved simultaneously. This is not always possible to do, even by numerical analysis, because it involves the resolution of several differential equations at the same time. This is the reason why the individual heat transfer coefficient, h, is defined as:

$$Q = h\ A\ (T_s - T_f) \tag{1.2}$$

Where Q is the heat flow from a fluid at a temperature of T_f, to a solid at T_s. The fluid and the solid are in contact by a surface equal to A. The heat transfer coefficient is an experimental coefficient, it depends of the material, the fluid conditions and the fluid dynamics like the density, velocity, viscosity or the surface geometry.

In a heat exchanger, the design equation (1.3) is:

$$Q = U\ A\ \Delta T_{lm} \tag{1.3}$$

Thermal radiation is the transfer of energy in the form of electromagnetic waves. Unlike conduction and convection, neither a material environment nor a temperature gradient are needed, since any body at a higher temperature than 0 K emits radiation. This radiation depends on the temperature of the source and vacuum conditions bring on its transmission. In the case of heat exchangers, radiation is negligible in comparison to conduction and convection.

1.2. **HEAT TRANSFER ENHANCEMENT TECHNIQUES**

As it has been mentioned before, the maximization of heat transfer is an important fact in order to design high-efficiency heat exchangers. Heat transfer enhancement techniques can be classified in three ways: active, passive and compound methods. Active methods require the input of external power, while passive methods doesn't. Referring to compound methods, as the name implies, they are a combination of both. (Zhang et al., 2016)

The following subsections are a summary of the most important techniques, in Appendix 1 there is a table with more specific examples and their TPFs.

1.2.1. Thermal Performance Factor

In order to decide if a modification is favourable to be applied in an industrial field, pressure drop and heat transfer enhancement need to be taken into account. To evaluate the effectiveness of a technique, the Thermal Performance Factor (TPF) is defined (1.4):

$$\eta = \frac{\frac{Nu}{Nu_0}}{\left(\frac{f}{f_0}\right)^{1/3}} \tag{1.4}$$

TPF represents the ratio of the relative effect of change in heat transfer rate to change in friction factor (Maradiya, Vadher, & Agarwal, 2017). Where Nusselt numbers (1.5.a) represent the importance of convection heat transfer in relation with heat conduction, and friction factors(1.5.b) refer to the pressure drop.

$$\text{(a)} \quad Nu = \frac{h\,l}{k} \qquad\qquad \text{(b)} \quad f = \frac{\Delta P}{(2\,\rho\,v^2)(l/D_h)} \tag{1.5}$$

The Thermal Performance Factor is also known as the overall enhancement ratio (OER). (Hasanpour, Farhadi, & Sedighi, 2014)

1.2.2. Active Methods

There are several kinds of active methods which can be classified into techniques where the channel walls are immobile, which act directly on the fluid, or into techniques where a solid wall is made to move periodically. (Léal et al., 2013)

The three most important methods regarding the first type are: electrohydrodynamics, consisting in coupling the electric field with a flow field medium which generates several forces in both single and two-phase flow, lead to physical mechanisms that enhance heat transfer. The other two methods consists in impinging a high speed fluid (jet) or droplets (spray) on a heated surface. (Léal et al., 2013)

In second place, the main techniques involving the use of movable walls where the heat transfer takes place are: acoustic waves generated by high frequency oscillations of a membrane; synthetic jet where the flow is imposed by the motion of diaphragm bounding cavity;

and dynamic deformation of a solid at high amplitude (Léal et al., 2013). All of those methods increase fluid mixing and boundary layer disruption, causing artificial convection.

1.2.3. Passive Methods

Passive methods, because of their nature are the most common heat transfer enhancement techniques. They produce two main effects: increasing the heat transfer surface and reducing the thermal boundary layer thickness by generating swirl flow neat the heat transfer surface.

Different techniques can be combined, so there is an infinity of possible pipe configuration. Next, there is a description of some methods frequently used, and Table A1.1, is a summary of some studied configurations and their TPF:

1.2.3.1. Swirl producing devices

The most used swirl producing devices are twisted tapes (tt), which performance depends on its dimensions, and twist ratio. There are other kind of inserts such as wire coil, helical screw inserts, wings, vortex generator pairs or wavy tapes.

Regarding the length of tt inserts it has been seen that only full-length pipes at low Re have TPF higher than unity (Eimasa-ard et al., 2009). As to the effect of space ratio, the heat transfer coefficient increases as twist and space ratios decrease (Maradiya et al., 2017). (Sarada et al., 2011) found that heat transfer enhances with the increase of the tt width, and according to (Esmaeilzadeh et al., 2014 the increase in thickness also increases the TPF. It has been seen that when twist ratio decreases leads to an enhancement in heat transfer, but the optimal configuration is an increasing-decreasing twist ratio (Maradiya et al., 2017).

Some of the most common modifications to tt are perforation, notched and jagged tt, the last ones having the higher TPF (Hasanpour et al., 2014), but when a jagged tt insert is compared with a butterfly insert, it doesn't have the best TPF (Shabanian et al., 2011). Another kind of modification to tt are wings, there have been analysed straight and oblique delta winglet along with twin delta winglet tt (Maradiya et al., 2017), the TPF depends on the inclination, depth and position of the winglet cutting, apart from the type of winglet. When the twisted tape is perforated, the TPF increases, because the pressure drop diminishes.

Instead of making modifications to the tt, inserting multiple tt is an option. (Eiamsa-ard, Nuntadusit, & Promvonge, 2013) found that counter-coupling tt have a higher TPF than co-coupling ones. (Vashistha, et al. 2016) worked with co-swirl and counter-swirl orientations with different number of tt inserts, and concluded that the counter-swirl orientation performed better than the co-swirl, and that four tt inserts give a higher TPF than one or two. (Maradiya et al., 2017)

Full length helical twisted tapes inserts improve heat transfer as well. There are different configurations based on their twist and pitch ratio, length and direction of the turns, and the combination of more than one insert. (Maradiya et al., 2017)

Coil wire inserts are a method to enhance heat transfer, its performance depends on its geometric characteristics, such as the shape of the cross section of the coil wire, pitch ratio, distance between the tube wall and the coil wire, wire diameter, if the insert is full-length or not. It is also possible to combine twisted tape with wire coil inserts. (Maradiya et al., 2017)

1.2.3.2. Surface characteristics

Modifications to the surface of the pipe can improve the heat transfer rate, by creating turbulence and because the heat transfer surface increases. There are different characteristics to be modified, for example roughness of the surface, addiction of fins or baffles or corrugation of the pipe wall.

Regarding vortex generators attached to the surface, it has been seen that geometric shape, angle of attack and placement of the vortex generator, as well as pair and wavy fin height can affect the heat transfer (Lotfi, et al. 2016). Different geometric fin characteristics can be used, studying different types of wings, (Zhang et al., 2016) and (Zdanski et al., 2015) concluded that winglet with delta shape perform better than helical or rectangular fins. (Zhai et al., 2019) found that upstream flow direction is better than downstream flow direction, and common-flow down performs better than common-flow up, when vortex generator pairs are used.

Artificial roughness can be added to the tube surface, either by adding periodic grooves or ribs to the surface or by coating it. The effect of ribs and grooves specially depends on its distribution along the pipe, shape and height (Maradiya et al., 2017). Micron scale coating,

which can be obtained by coating or machining, promotes turbulence and it is one of the most important factors for boiling heat transfer (Zhang et al., 2016). Nanoscale coating, which can be produced by coating, etching, painting or directional growth, change physical and chemical properties. It has little effect in single phase heat transfer, but it can improve phase change processes because it increases the nucleation sites due to the presence of gas trapped in the coating pores (Zhang et al., 2016).

Corrugation of the pipe is another method to enhance heat transfer. Depending on height and angle of the crest, a corrugated pipe promotes turbulence apart from having extended surface.

1.2.3.3. Tube geometrics

The two principal tube parameters to vary are the duct shape and the tube shape. (Khoshwaght-Aliabadi & Arani-Lahtari, 2016) concluded that all twisted channels with different duct shapes (squared, semi-circular) performed better than a smooth circular pipe. (Petkov et al., 2014) resolved that hexagonal duct performed best among isosceles triangular, rectangular, trapezoidal and elliptical shapes (Maradiya et al., 2017). There are other configurations, such as twisted oval or twisted tri-lobed tubes (Tang, Dai, & Zhu, 2015).

As to the tube shape, (Khoshwaght-Aliabadi et al., 2015) obtained the better performance for helical tube, followed by spiral and serpentine tubes. (Maradiya et al., 2017)

1.2.3.4. .Fluid modifications

Nanoparticles in suspension in a fluid improve the apparent thermal conductivity, but it also increases the pressure drop. It has been seen that the TPF increases with lower weight fractions and increase in flow rate (Kumar & Amano, 2015). The effect of nanofluid depends on the flowing fluid/particle convination as well. (Maradiya et al., 2017)

The last example to improve the TPF is to use phase change of the circulating fluid. On one hand, there is hydrodynamic cavitation, vapour or air nucleus development due to local static pressure reduction below a critical value (Zhang et al., 2016). This phenomenon enhances heat transfer because the bubles mix the fluid, reducing the thickness of the boundary layer. On the other hand, condensation can be used, because the thin liquid layer enhances heat transfer.

1.3. **CFD**

1.3.1. Transport equations

In this project numerical analysis is used to solve microscopic balances. Mass, energy and momentum are conserved variables in a system, in order to describe the fluid dynamics the three laws of conservation need to be solved.

The mentioned conservation laws can be cast as a general transport equation (1.6), which is solved by the software. (Date, 2009)

$$\frac{\partial(\rho\,\Phi)}{\partial t} + \nabla[\rho\,\vec{u}\,\Phi] = \nabla\left[\Gamma_{eff}\,\nabla\Phi\right] + S_{\Phi} \tag{1.6}$$

The meaning of Φ and Γ_{eff} depends of the transported property, see Table 1.1 for each property correspondence. The time derivative is the accumulation term, representing transient state and the second term refers to convection. At the other side of the equal there is a net source term (S_{Φ}) that can include different sources or forces, and the one referring to molecular conduction.

Table 1.1. General transport equation correspondence with individual equations.

Equation	Transported property	Φ	Γ_{eff}	S_{Φ}
1.5	Global mass	1	0	0
1.6	Momentum	$\vec{v}$	μ_{eff}	$-\nabla p + \rho\,\vec{g}$
1.7	Temperature (energy)	T	k_{eff}/C_p	Q'''/C_p

This equations can be used as far the continuum hypothesis is considered. It means that during the resolution of the equations, there are enough molecules in between two nodes for the matter to be considered continuous.

1.3.1.1. Transport of mass

The law of conservation of mass states that the difference between the rate of mass in and out is equal to the rate of mass accumulation (Date, 2009). This statement is equivalent to the

global mass balance. For a single component fluid, in a derivative form it can be written as in equation 1.7, where the first term represents the mass accumulation and the second one represents the net inflow.

$$\frac{D\rho}{Dt} = -\rho\ (\nabla \cdot \overrightarrow{u}) \tag{1.7}$$

When a mass balance is applied to a single species it can appear a net source term, in addition, Fick's law of mass diffusion is taken into account.

1.3.1.2. Transport of momentum

The law governing transport of momentum is Newton's second law of motion, which affirms that for a given direction, the rate of accumulation of momentum is equal to the difference between the rate of momentum in and out plus he summation of forces acting on the control volume. (Date, 2009)

For Newtonian fluids, Newton's second law of motion, combined with Stokes's stress laws lead to Navier-Stokes equation 1.8:

$$\rho\ \frac{D}{Dt}\vec{u} = -\nabla p + \ \mu_{eff}\ \nabla^2\vec{u} + \ \rho g \tag{1.8}$$

The term at the left side of the equal represents the accumulation of momentum, the first term at the right side refers to the pressure gradient, the second is the friction term and the last one represents gravity force effect. (Date, 2009)

The reason why μ_{eff} is used instead of μ, is to take turbulence into account. The effective viscosity concept, $\mu_{eff} = \mu + \mu_t$, is also known as Boussinesq assumption. It is important to mention that viscosity is a property characteristic of the fluid, whereas, the turbulent or Eddie viscosity is a primarily property of the flow. (Bird, Stewart, & Lightfoot, 2002)

1.3.1.3. Transport of energy

Transport of energy is governed by the first law of thermodynamics, which states that: the rate of change of energy of the control volume is equal to the sum of the net rates of energy transferred by convection and conduction, plus the net volumetric heat generation within the control volume, and the net rates of work done by surface and body forces. (Date, 2009)

A possible way to give the energy transport equation is in the form of an enthalpy balance combined with Fourier's law of heat conduction. This equation can be expressed as a function of temperature ($h = C_p(T - T_{ref})$), as shown in equation 1.9.

$$\frac{\partial(\rho\,\mathrm{T})}{\partial t} + \nabla[\rho\,\vec{u}\,\mathrm{T}] = \nabla \cdot \frac{k_{eff}}{c_p}\,\nabla\mathrm{T} + \frac{Q'''}{c_p} \tag{1.9}$$

The two terms left of the equal are the accumulative and convective terms respectively. Straightaway there is the term representing the transfer via conduction and, at last the net source term.

1.3.2. Turbulence models

Even though there is not a satisfactory definition of turbulence yet, when there are large velocity gradients, the flow goes from laminar to turbulent. *An outstanding feature of turbulent flow, as opposite to laminar flow, is that molecules move in chaotic fashion along complex irregular path.* The strong chaotic motion causes the various layers of fluid to mix together intensively. (Sadrehaghighi, 2019)

A turbulent flow is characterized for being disorganized, chaotic and seemingly random. It is sensible to initial conditions and present an extremely large range of length and time scales, always satisfying the continuum hypothesis. It enhances mixing and energy dissipation. Other characteristics are three dimensionality, time dependence, rotationality and intermittency in time and space. (McDonough, 2007)

The complexity of this phenomenon makes the use of statistical models necessary. Turbulence modelling has the aim to develop equations that will predict the time-averaged velocity, pressure, and temperature fields without calculating the complete turbulent flow pattern as a function of time (Sadrehaghighi, 2019). From more computing power requirements, needed by DNS (Direct Numerical Simulation) which does not use any turbulence model to solve the Navier-Stokes, to less, there are LES and RANS models.

1.3.2.1. RANS

The Reynolds Average Navier-Stokes equations are obtained from decomposing dependent variables of the N-S equations 1.10, with the Reynolds decomposition 1.11, into time mean and

fluctuating components. Equation 1.12 is a common way to express RANS equations. (McDonough, 2007)

$$\text{(a)} \quad \nabla U = 0 \tag{1.10}$$

$$\text{(b)} \quad U_t + U \cdot \nabla U = -\nabla \mathrm{P} + \upsilon \Delta \mathrm{U} \tag{1.10}$$

$$U = \bar{u} + u' \tag{1.11}$$

Where $\bar{u}$ is the time average, therefore is independent of time.

$$\bar{u_t} + \nabla \cdot \bar{u}^2 = -\nabla \bar{p} + \upsilon \Delta \bar{u} - R(u', u') \tag{1.12}$$

Where
$$R(u', u') = \begin{pmatrix} \overline{u'^2} & \overline{u'v'} & \overline{u'w'} \\ \overline{u'v'} & \overline{v'^2} & \overline{v'w'} \\ \overline{u'w'} & \overline{v'w'} & \overline{w'^2} \end{pmatrix} \tag{1.13}$$

There are different RANS models that permits to solve the equation. They can be classified in linear and non-linear. Linear, or first order models, directly use the Boussinesq assumption, and the mean velocity field is related with the mean turbulence fields by the eddy viscosity coefficient in a linear relationship. Moreover, linear models are characterized by the number of equations used, being the two equations models the most popular. Non-linear, or second order models, use the effect of closure to the Reynolds equation with a non-linear relation between the main mean fields. (Sadrehaghighi, 2019)

Straightaway, some specific models are mentioned. Two equation linear models can be differentiated into two families, k-ε and k-ω. k-ε models permit to construct eddy viscosity without needing to appeal to experimental data, k refers to the equation for turbulent kinetic energy, and ε represents equation for the dissipation rate of turbulent kinetic energy, where ε is the length scale for small eddies. This model is widely used because it has good convergence rate and doesn't have very memory requirements, but it is not very accurate for jet flows, for adverse pressure gradients or flows with strong curvature. (Sadrehaghighi, 2019).

k-ω models also use the equation for turbulent kinetic energy k, but instead of ε, it solves ω, the turbulence frequency. They are more advantageous in comparison with k-ε models, especially for integrating through the viscous sub-layer, and in flows with adverse pressure gradients. (Sadrehaghighi, 2019).

The k-ω SST (Shear-Stress-Transport) includes transport effects to the eddy-viscosity formulation, this gives more accurate predictions for flow separation under adverse pressure gradients, because it better calculates flow in the near-wall region. The Standard k-ω, or Wilcox k-ω model, solves the two equations k and ω where the stress tensor is computed from the eddy viscosity concept, it is also known by its sensibility to freestream conditions. To solve this problem, the BSL (Baseline) k-ω model was developed. It is a blend between k-ε for the outer regions and k-ω near the surface. (Sadrehaghighi, 2019).

ANSYS Fluent © also presents the GEKO k-ω (Generalizes k omega) model, which is more easily calibrated to the flow and can be used for a wide range of applications. (Menter Florian, 2019)

1.3.2.2. LES

LES, or Large-Eddy Simulation, requires modelling of art of the inertial subrange and into the beginning of the dissipation scales. The amount of required modelling is set by the amount of resolution that can be afforded. (McDonough, 2007)

It reduces the computational costs by ignoring the smallest length-scales, which are not irrelevant. So large motion is calculated, while the small-scale motion needs to be modeled. (Sadrehaghighi, 2019)

The classical approach to LES consists on decomposing flow variables into large- and small-scale parts, with the large-scale part purportedly defined by a filtering process; filtering the governing equations and substituting the decomposition into the non-linear terms to construct the unclosed terms to be modelled and obtain a system of equations for resolved-scale variables. Before solving the equations for the large-scale contribution, the unsolved stresses need to be modeled. (McDonough, 2007)

2. OBJECTIVES

The aim of this project is to analyse heat transfer in a pipe with a twisted tape insert and corrugated surface by making CFD simulations with ANSYS Fluent ©.

More specifically, the results obtained with CFD will be compared with experimental data in order to verify their reliability. The effect of the pipe and twisted tape geometrics in heat transfer enhancement will be found. Finally it will be calculated the Thermal Performance Factor in order to consider the effectiveness of the modification, taking pressure drop into account.

3. METHODS AND SETUP

There has been used a virtual workstation with 16 CPU, equivalent to a memory of 62,5 GB, accessed through a remote desktop.

All CFD simulations have been done using ANSYS Fluent © and pipe geometrics have been drawn with Design Modeller ©.

3.1. PIPES DESCRIPTION

The pipes that have been simulated in this project correspond exactly with the ones experimentally studied by (Chamarro Aguilera, 1988). Not all the pipes that were studied experimentally have been studied numerically, a representative selection of geometric factors has been done.

The original pipes in a heat exchanger from a combustion gases chimney were made of steel and pipes without any modification. They tended to fail at the inlet, where the temperature was significantly lower, because of the corrosion caused by acidic condensations of gases like SO_2.. The material of the pipes is PTFE (Polytetrafluoroethylene), also known as Teflon. It was chosen despite its low thermal conductivity because it is resistant to corrosion and is able to operate at high temperature. PTFE mechanical properties and corrugation of the pipe makes them flexible, on one side, this, and the non-stick properties of Teflon, helps to prevent incrustation of dirt. On the other side, it could cause the flexing of the pipe. To avoid it, steel twisted tape were inserted to the pipes, helping to distribute the fluid through the pipe.

The Figure 3.1 represents a drawing of the pipes, and shows the characteristics used to define them:

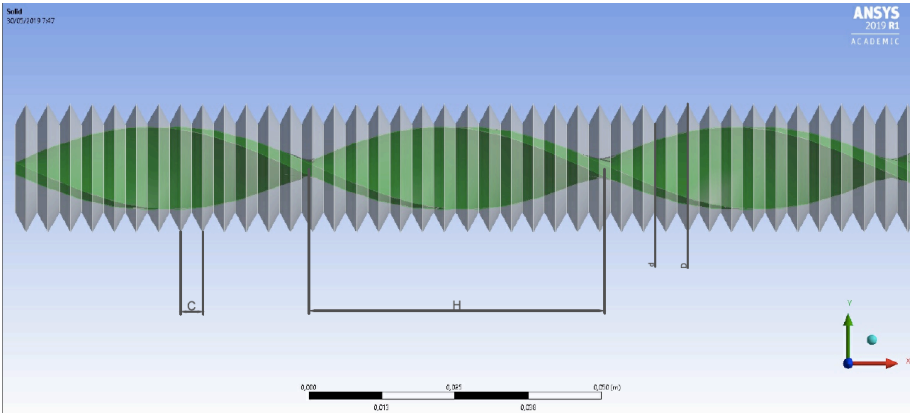

Figure 3.1. Part of the drawing of pipe 1A.

The length (L) of the pipes is 80 cm and the thickness of the twisted tape is 2 mm. The rest of dimensions, which vary depending on the pipe are specified in Table 3.1, where N is the number or crests.

Table 3.1. Pipes dimensions.

Pipe	D [mm]	d [mm]	N	H [mm]	ttW [mm]
1A	23	15	212	50	14
1B	23	15	212	104	14
1D	23	15	212	222	14
2C	27	15	158	150	14
3C	30	17	161	173	16
4A	38	25	182	108	24
4B	38	25	182	204	24
5C	50	29	128	298	28
7D	70	35	99	410	34

It is important to consider that D represents an external diameter, while d is an intern diameter. The drawing of the pipes and the data treatment have been done using the internal diameter of the pipe, that means that Teflon thickness has been subtracted from D values of Table 3.1.

When calculating the heat transfer surface, crest have been treated as wings, therefore, the transfer area has been calculated as a plain tube of internal diameter d, and external diameter d + 1mm.

3.1.1. Teflon thickness

Real Teflon pipes are considered to be 0.5 mm thick, this is a small scale, so its precision is questionable. For this reason, different wall thickness, between 0.3 mm and 0.6 mm, have been studied for experiment 1 of the pipe 4A, which represents a medium-sized pipe.

The most similar outlet temperature results to experimental data, were obtained with wall thickness of 0.35 mm and 0.5 mm, with a 4 ºC difference in both cases. Pressure drop results were more similar to experimental results with 0.5 mm (5.0% difference versus 9.3% difference with 0.35 mm wall thickness). Go to Appendix 3 to see the obtained results.

External wall thickness was set as a boundary condition in ANSYS Fluent © setup, instead of drawn.

3.2. DIMENSIONLESS NUMBERS

To contrast the performance of each pipe, the individual heat transfer coefficient and the Fanning friction factor are analysed for each data set. These numbers depend on the fluid physical properties, the flow and the pipe characteristics.

Pipe geometric characteristics studied in this project are the pipe diameter, the height and width of the crests, and the twisted tape curvature. In order to typify the pipes three dimensionless quantities have been defined as:

$$\text{(a) } N1 = \frac{D}{d} \qquad \text{(b) } N2 = \frac{H}{d} \qquad \text{(c) } N3 = \frac{C}{d} \tag{3.1}$$

The number of crests is bounded to the external diameter of the pipe, so for each pipe N1 and N3 are constant, and there are not any pipes with the same N1 and different N3, nor in reverse.

In order to reduce the number of variable regarding the fluid and flow characteristics, the usual dimensionless quantities are used (3.2). The Reynolds number gives a notion of the flow turbulence, the Nusselt number shows the convective heat transfer in comparison with the

conductive one. Finally the Prandtl number gives the ratio between momentum and thermal diffusivities.

$$\text{(a) } Re = \frac{\rho\, v\, d}{\mu} \qquad \text{(b) } Nu = \frac{h\, d}{k} \qquad \text{(c) } Pr = \frac{C_p\, \mu}{k} \tag{3.2}$$

3.3. **ANSYS SETUP**

Next subsection describe the parameters used in all the simulations run. All the variables that are not mentioned were set up as ANSYS default.

3.3.1. Meshing

The meshing of the pipes was made with ANSYS meshing tool. In order to obtain valid results the mesh must not affect to the result, to assure this condition, a small research of different meshes was made (see 4.1. subsection).

At this point velocity inlet and pressure outlet surfaces were designated, as well as external wall and tt wall surfaces groups.

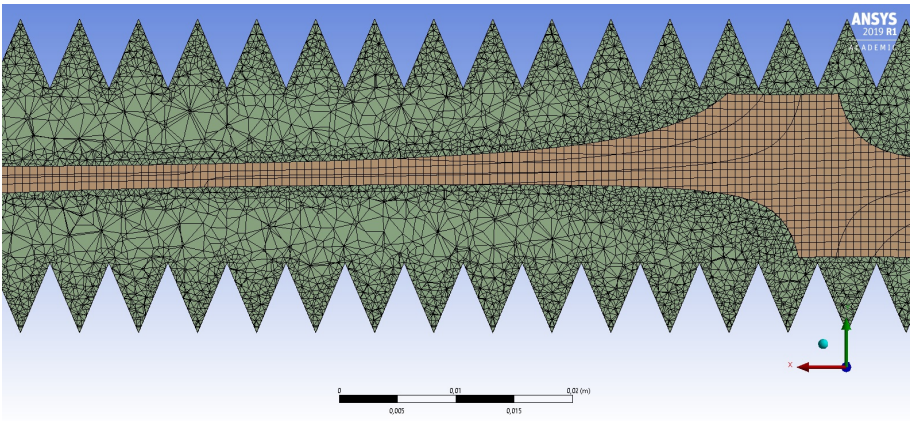

Figure 3.2. Mesh example. Pipe 2B, 1.1 million nodes.

3.3.2. ANSYS Fluent ©

Gravity effect was neglected because both the direction of the flow and the pipe orientation are horizontal. The type of Solver used was Pressure-Based in steady time.

Materials setup considered the following properties for air, Teflon and steel.

Table 3.2. Material properties setup.

Air[(b)]	Thermal Conductivity (W/(m·K))	$0.00477 + 7.2 \cdot 10^{-5}\ T$
	Viscosity (kg/(m·s))	$4.85 \cdot 10^{-6} + 4.53 \cdot 10^{-8}\ T$
	Specific Heat (J/(kg·K))	$737.815 - 0.17935\ T + 3.78 \cdot 10^{-4}\ T^2$
	Density (kg/m^3)	Ideal-gas[(d)]
Teflon[(c)]	Thermal Conductivity (W/(m·K))	0.25
	Specific Heat (J/(kg·ºC))	970
	Density (kg/m^3)	2100
Steel[(d)]	Thermal Conductivity (W/(m·K))	16.27
	Specific Heat (J/(kg·K))	502.48
	Density (kg/m^3)	8030

(a) Temperature (T) in K
(b) Properties estimated from (The Engineering ToolBox, n.d.-a), 21.03.2019.
(c) Properties estimated from (The Engineering ToolBox, n.d.-c)], 04.04.2019.
(d) Default properties from ANSYS database

The fluid at the exterior of the pipe in experimental data, was water vapour. Therefore, the external wall boundary condition is type one, the temperature is constant throughout time and space. Velocity and temperature inlet were set as boundary conditions, as well as the pressure outlet. This was set to 0.0001 Pa, in order to work with relative pressures, it was not set to 0 Pa, because the program would not be able to solve the model.

3.3.2.1. Models

The simulations were run with Energy equation on, and turbulent model. The turbulence model chosen was k-ω SST (see 4.2. subsection) with default set for all parameters.

3.3.2.2. Solution methods

Convergence absolute criteria was set to 10^{-4} for all residuals except for the energy equation one, which was set to 10^{-6}. The solution method used was Coupled (with the default setup), and when necessary to reach convergence, SIMPLE method with the Pressure Pseudo-Transient Explicit Relaxation Factor between 0.3 and 0.7 was used. Turbulent kinetic energy spatial discretization was set to second order upwind.

In some cases, continuity, k and omega residuals were impossible to lower to 10^{-4}. In those cases, a solution was considered converged when all the residuals were $<10^{-3}$.

Continuity residuals of pipe 1A, which has the most twisted twisted tape, did not get to 10^{-3} with any solution method. For this reason, a different approach, with a more dense mesh was tried (see 5.5 subsection).

4. MESH AND MODEL RESEARCH

4.1. MODEL

To choose which turbulence model to use, some of the most common RANS models were compared for the data set 2 of pipe 4B. Graphic 4.1 shows that the model giving the closest results to experimental data is k-ω SST.

Charts 4.1. (a) Temperature outlet (a) and pressure drop (b) experimental and CFD results for pipe 4B-2 and different turbulence models.

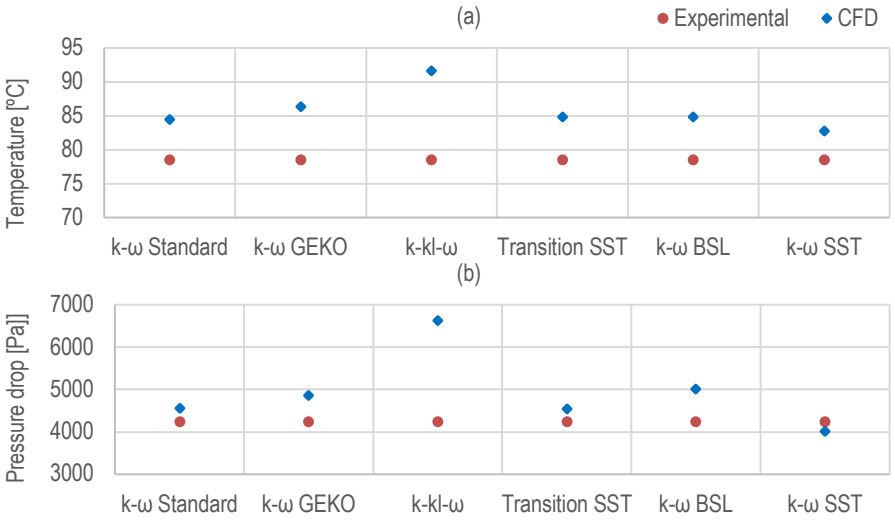

4.2. MESH

The maximum workable number of nodes is around 4 million. Different meshes, with varying number of nodes have been tested for experiment 2 of pipe 4B, which represents a medium-sized pipe with a middle Re number. The mesh parameters modified were Element Size

(between 6·10-3 m and 5·10-4 m), Growth Rate (between 1.2 and 2.0) and Smoothing was set to high. Different Max Size were tried, but no significance number of nodes nor orthogonal quality differences, were observed. Graphics 4.2 (a) and (b) show the results obtained with CFD in comparison with the experimental ones.

Charts 4.2. (a) Temperature outlet (a) and pressure drop (b) experimental and CFD results for pipe 4B-2 and different number of nodes.

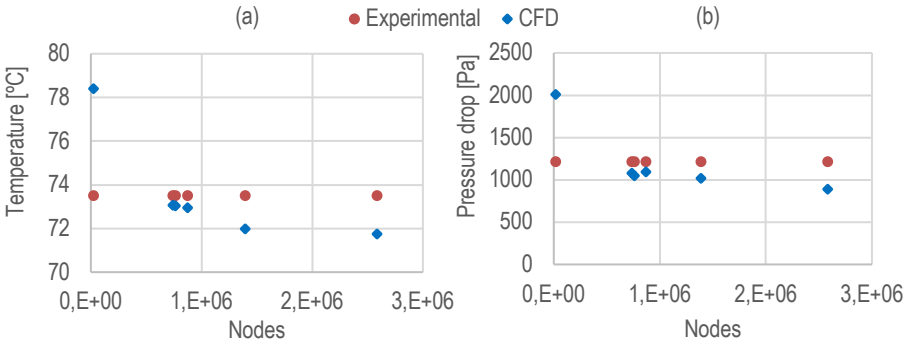

The best similitudes were obtained with a number of nodes between 0.7 and 1.4 million. For this reason, further simulations were set so that the number of nodes was located between 1.0 and 1.5 million.

5. RESULTS AND DISCUSSION

5.1. COMPARISON WITH EXPERIMENTAL DATA

In order to confirm that the chosen ANSYS setup is valid, the temperature outlet and the pressure drop obtained with CFD are compared to the experimental values.

Chart 5.1. Experimental and CFD temperature outlet results for every set of data.

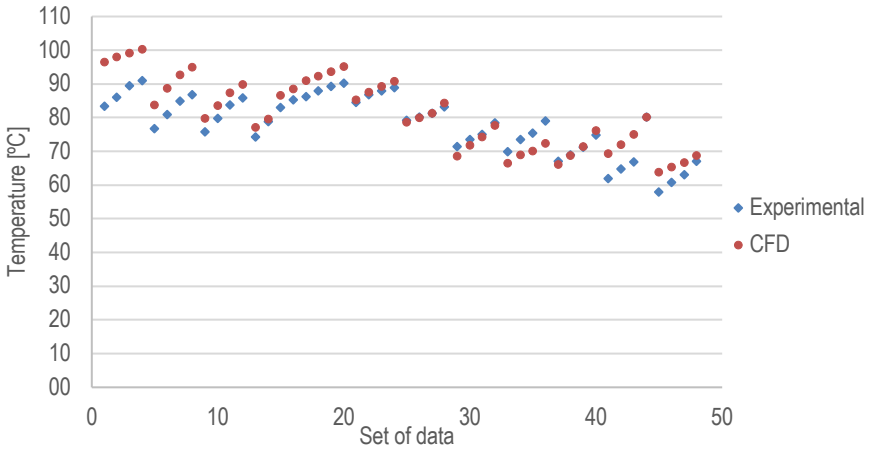

Chart 5.1 shows the difference between the temperature outlet results obtained with CFD and the available experimental data. In most of cases the results obtained with CFD are higher than the experimental data. The maximum deviation is 13.0ºC, which represents 16% error, but the average deviation is 4.0ºC, with an average error of 5%.

Chart 5.2. Experimental and CFD pressure drop results for every set of data.

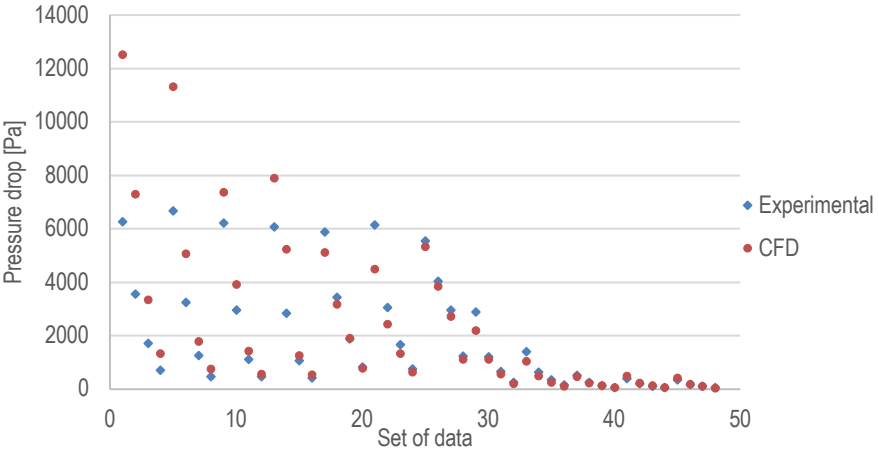

Chart 5.2 exposes the differences between experimental and CFD results for pressure drop. The maximum absolute error is 6259 Pa, which represents 100% relative error, but the larger error is 105%, with an absolute value of 3725 Pa. The errors for pressure drop are concededly more important than the temperature ones, the cause of this is that the energy equation is easier to solve than the turbulence models, besides, those models are simplifications of the transport equations.

5.2. GEOMETRIC CHARACTERISTICS EFFECT ON HEAT TRANSFER

The effect of the pipe characteristics on heat transfer was analyzed by comparing Nusselt numbers of selected pipes at different Reynolds. The individual heat transfer coefficients were calculated from equaling equations 1.2 and 1.3 and the fluid properties at the mean temperature.

5.2.1. N1

In the first place, to see how crests height affects to heat transfer enhancement, pipes with constant N2 (H/d) and N3 (C/d) were chosen, while varying N1 (D/d). There aren't any pipes with the same N2, and the fact that N1 and N3 are bounded, make that N2 and N3 are not exactly equal for the chosen pipes.

Chart 5.3. Nusselt values in front of Reynolds at N2 = 6.98 ± 0.03 and N3 = 0.23 ± 0.02.

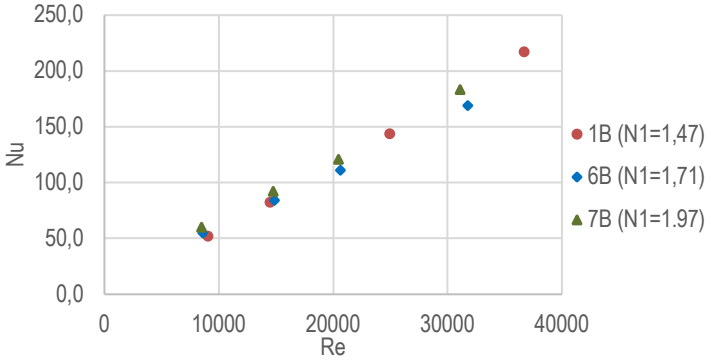

Chart 5.3 does not show a clear relation between N1 and the enhancement of heat transfer due to convective transport.

5.2.2. N2

Secondly, to see the influence of the twisted tape twist pitch, pipe 1 with different tt inserts are compared. In this case N1 and N3 are exactly the same, because the pipe itself does not change.

Chart 5.4. Nusselt values in front of Reynolds at N1 = 1.47 and N3 = 0.25.

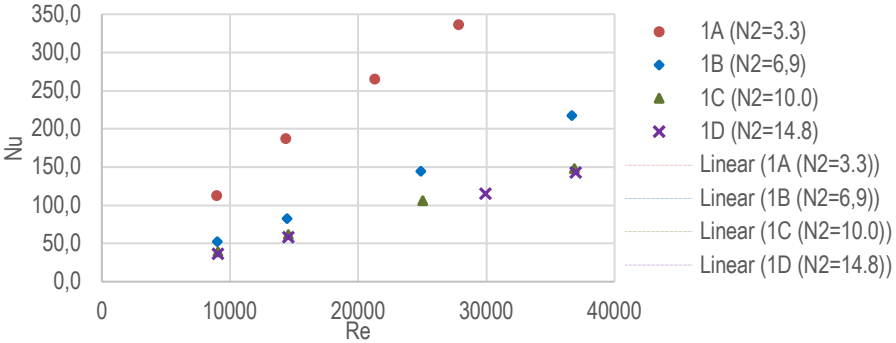

Chart 5.4 shows that when N2 increases, Nusselt number decreases, meaning that convective heat transfer loses importance in front of conductive transfer. Lower N3 equal to more twisted tt. These results have since, since the twist promotes turbulence, which in turn reduces the fluid boundary layer, enhancing heat transfer.

5.2.3. N3

Finally, in the case of the width of the crests, it happens the same as in N1 case. Pipes with different N3 and similar N1 and N2 were chosen, but it is impossible to compare pipes with exactly the same N1 and N2.

Chart 5.5. Nusselt values in front of Reynolds at N1 = 1.71 ± 0.02 and N2 = 10.2 ± 0.1.

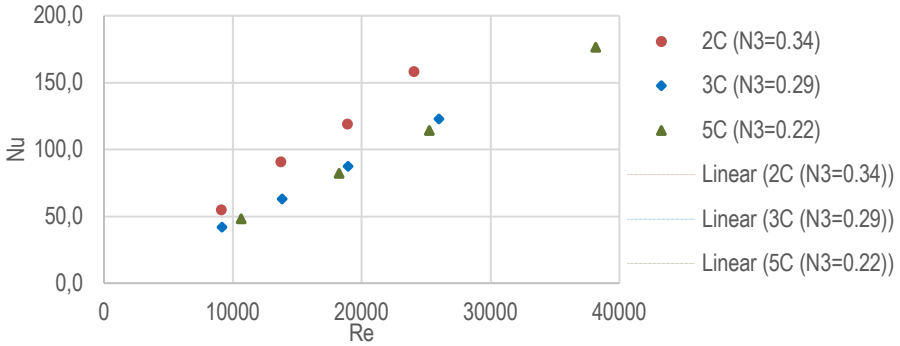

In the chart 5.5, appears as if Nusselt number increases with the value of N3, meaning that as less crests, the convective heat transfer phenomena increases.

One way to avoid the variability of N1 and N3 is to compare different pipes with the same tt insert. This situation only occurs with pipes 1 & 2 and 6 & 7. Chart 5.6 shows how Nu augments when the crests of the pipes become larger, both in height and width. (See Appendix 4 for more charts)

Chart 5.6. Nusselt values in front of Reynolds for pipes 6 & 7 B (N2 = 7.0).

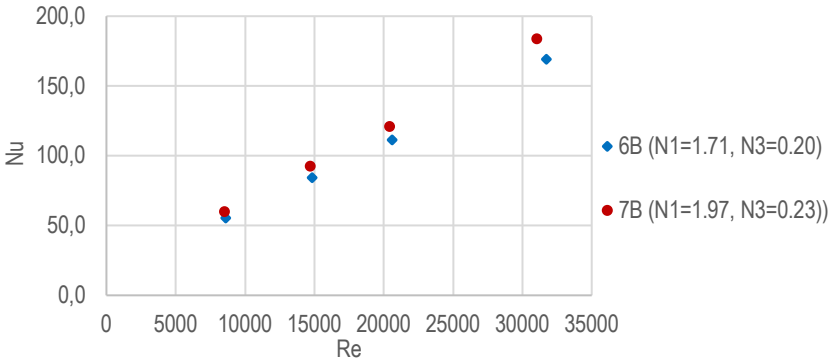

5.2.4. Nusselt correlation with pipe geometry

This subsection pretends to find the coefficients relating the previously defined dimensionless numbers of the equation 5.4.

$$Nu = A' \, Re^{B} \, N1^{C} \, N2^{D} \, N3^{E} \, Pr^{F} \tag{5.1}$$

Prandtl number is constant for all the sets of data, with a value of 0.51 for both experimental and CFD obtained data. For this reason equation 5.1 can be simplified to equation 5.2.

$$Nu = A \, Re^{B} \, N1^{C} \, N2^{D} \, N3^{E} \tag{5.2}$$

Linearizing equation 5.2, function 5.3 is obtained.

$$\log Nu = A + B \log Re + \; C \log N1 + \; D \log N2 + E \log N3 \tag{5.3}$$

The coefficients are found with multivariable lineal regression, which has been adjusted separately for experimental results and CFD results. In the experimental results analysis, all available data has been used, even if the matching CFD simulation was not done. Tables 5.1 and 5.2 show the values obtained.

Table 5.1. Lineal regression results for CFD results.

	Coefficient	Standard error	CI 95%	Pearson correlation coefficient
A	-1.43	0.15	-1.72 – -1.13	
B (Re)	0.982	0.031	0.918 – 1.054	0.830
C (N1)	0.19	0.14	-0.10 – 0.48	-0.134
D (N2)	-0.791	0.042	-0.877 – -0.704	-0.431
E (N3)	0.132	0.083	-0.116 – -0.034	-0.075
			R 0.983	
			R² 0.966 ± 0.045	
			RSS 2.49	

Table 5.2. Lineal regression results for experimental data.

	Coefficient	Standard error	CI 95%	Pearson correlation coefficient
A	-2.32	0.13	-2.58 – -2.06	
B (Re)	0.975	0.028	0.918 – 1.031	0.914
C (N1)	0.53	0.14	0.26 – 0.81	-0.038
D (N2)	-0.291	0.030	-0.350 – -0.231	-0.164
E (N3)	-0.408	0.066	-0.538 – -0.277	-0.265
		R	0.963	
		R^2	0.927 ± 0.060	
		RSS	4.81	

It has been found a linear adjustment for both data sets with a correlation factor over 0.9, which means the adjustment is admissible. Moreover, the coefficients sets are similar, in both cases, the most influential variable is the Reynolds number, even when the fact that N3 is <0, what makes it takes importance with lower exponents, is considered.

An important difference is the value of N3 coefficient, the adjustment to experimental data shows an inversely proportional relation with the Nusselt number, unlike the adjustment to CFD results, where the relation is directly proportional. This can be caused by the fact, already exposed, that in the pipes used, N3 and N1 are bonded to each other. It is also remarkable the difference in N2 coefficient.

If the 95% confidence intervals are taken into account, the following equations 5.4 are obtained: (5.4)

(a) CFD $Nu = (-1.4 \pm 0.3) \cdot Re^{0.98 \pm 0.06} \cdot N1^{0.2 \pm 0.3} \cdot N2^{-0.79 \pm 0.09} \cdot N3^{0.1 \pm 0.2}$

(b) Experimental $Nu = (-2.3 \pm 0.3) \cdot Re^{0.97 \pm 0.06} \cdot N1^{0.5 \pm 0.3} \cdot N2^{-0.29 \pm 0.06} \cdot N3^{-0.4 \pm 0.1}$

A shortened way to write them is:

(a) CFD $Nu = -1.4 \cdot Re^{0.98} \cdot N1^{0.2} \cdot N2^{-0.79} \cdot N3^{0.1}$ (5.5)

(b) Experimental $Nu = -2.3 \cdot Re^{0.97} \cdot N1^{0.5} \cdot N2^{-0.29} \cdot N3^{-0.4}$

Confidence intervals permit to approximate B and C as equals, while, the rest of coefficients are the same order, but significantly different, which means, more pipes with different N2 and N3 values should be tested.

The order of the Re term is approximately 1, which means that the Reynolds number relation with the Nusselt is lineal, this is also visible in graphics 5.3 to 5.6.

The adjustment of these equations can be used to see which are the most important variables to increase convective heat transfer. They can also be applied to set the direction towards the heat transfer optimization of pipes.

5.3. GEOMETRIC CHARACTERISTICS EFFECT ON PRESSURE DROP

The effect of the pipe characteristics on pressure drop was analyzed by comparing fanning friction factor values of selected pipes at different Reynolds. The Fanning friction factor values were calculated from a mechanical energy balance in the form of equation 1.5.b. In this subsection, only CFD results will be analyzed.

5.3.1. N1

To see the effect of geometric characteristics of the pipe on pressure drop, the same pipes used for the heat transfer analysis have been chosen. To compare different crest height 1B, 6B and 7B at different Reynolds are represented in Chart 5.7.

Chart 5.7. f values in front of Reynolds at N2 = 6.98 ± 0.03 and N3 = 0.23 ± 0.02.

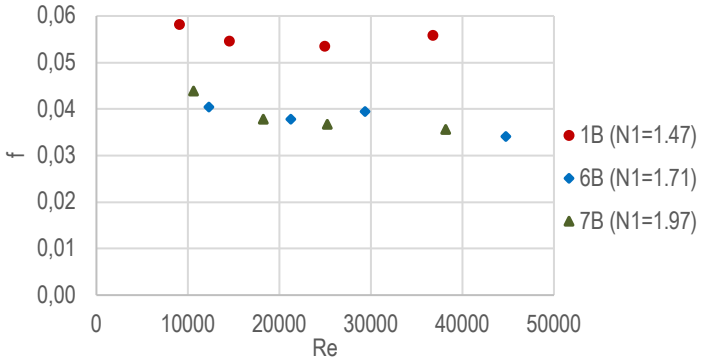

Chart 5.7 shows how the Fanning friction factor does not vary linearly with the Reynolds number. It can also be observed an increasing tendency of f when N1, the ratio between D and d decreases.

5.3.2. N2

Regarding the influence of the twisted tape, pipe 1 with different tt inserts are represented in Chart 5.8. It shows a similar tendency as for the Reynolds influence to chart 5.7. Regarding the effect of tt twist, the Fanning friction factor increases when the insert becomes more contorted. This is caused by the energy dissipated by the fluid movement in the radial axis and local swirls produced by the augment of turbulence.

Chart 5.8. f values in front of Reynolds at N1 = 1.47 and N3 = 0.25.

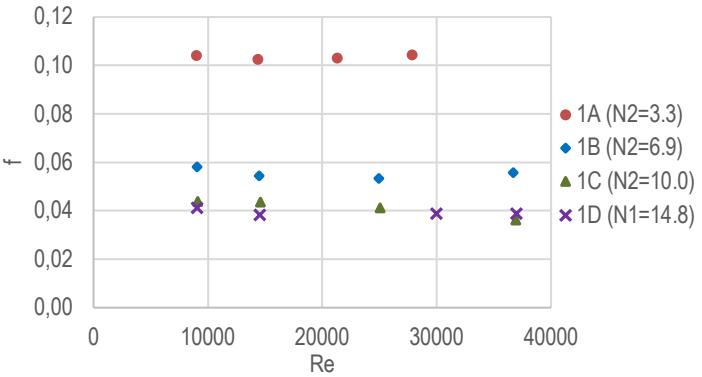

5.3.3. N3

As the pipes used are the same, N3 and N1 are bonded, and there is some variability in N1 and N2. Chart 5.9 represents how f varies with Re for pipes 2C, 3C and 5C.

Chart 5.9. f values in front of Reynolds at N1 = 1.71 ± 0.02 and N2 = 10.2 ± 0.1.

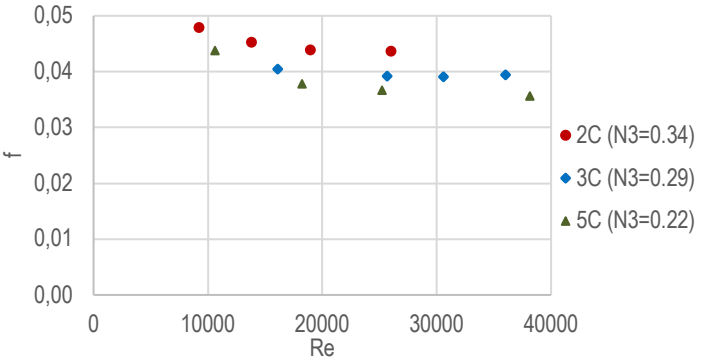

In this case, f values increase when the width of the crests also increases. This means that when the number of crests is lower, the pressure drop augments. A priori it does not have any intuitive explanation.

In order to counteract the relation between N1 and N3, different pipes with the same tt insert are compared in Chart 5.10. (see Appendix 4 for more cases)

Chart 5.10. f values in front of Reynolds for pipes 1 & 2 C (N2 = 10.0).

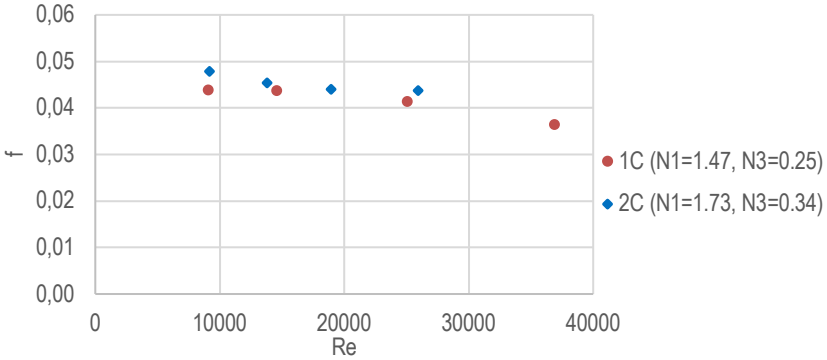

Chart 5.10 exposes how larger crests produce more pressure drop than smaller ones. This can be caused by the fact that in bigger crests, there is more fluid halted in comparison with smaller and softer crests.

5.3.4. Fanning friction factor correlation with pipe geometry

Initially the same treatment as heat transfer case was done for pressure drop results. Tables 5.3 and 5.4 show how there is not any exponential relation between the Fanning friction factor and the dimensionless numbers Re, N1, N2 and N3.

Table 5.3. Lineal regression results for CFD results.

	Coefficient	Standard error	CI 95%
A	0.14	0.13	-0.12 – 0.39
B (Re)	-0.115	0.028	-0.171 – 0.060
C (N1)	-0.42	0.13	-0.64 – -0.16
D (N2)	-0.659	0.037	-0.734 – -0.583
E (N3)	0.448	0.072	0.302 – 0.594
	R	0.952	
	R^2	0.898 ± 0.040	
	RSS	0.663	

Table 5.4. Lineal regression results for experimental data.

	Coefficient	Standard error	CI 95%
A	-0.19	0.20	-0.59 – 0.21
B (Re)	-0.182	0.044	-0.269 – -0.094
C (N1)	0.16	0.22	-0.27 – 0.59
D (N2)	-0.340	0.046	-0.432 – -0.247
E (N3)	0.10	0.10	-0.10 – 0.31
	R	0.663	
	R^2	0.418 ± 0.094	
	RSS	0.708	

Even though CFD results present a much higher correlation coefficient R^2, it is not >0.9 enough to be considered correlated, so the adjustment is not acceptable. The difference of R^2 values in CFD and experimental data, could be due to the greater number of pipes taken into account with experimental results, in comparison with the carefully selected pipes used in CFD simulations.

Because of the invalidity of approximating an equation to estimate f value as an exponential function of Re and the geometric dimensionless numbers, a set of charts for different pipes have been represented. Charts 5.11 to 5.18 emulate Moody diagrams where the twist of the tt insert is represented instead of the surface roughness. Representing a specific chart for a different pipe is plausible because of the relation between N1 and N3, which are constant for every pipe.

Chart 5.11. CFD f values in front of Re for pipes 1 (N1 = 1.47, N3 = 0.25).

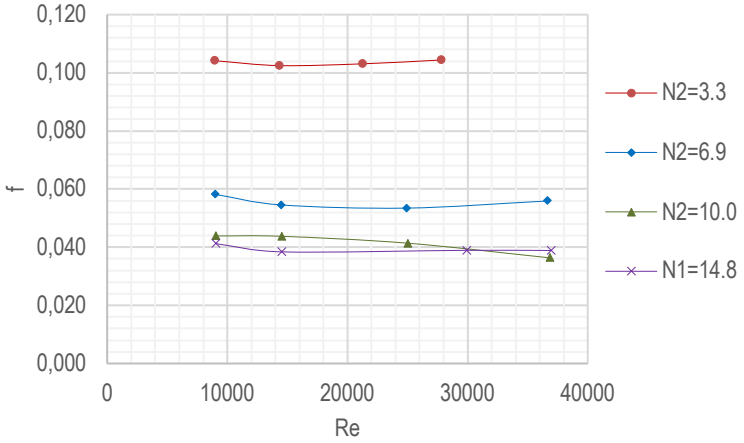

Chart 5.12. Experimental f values in front of Re for pipes 1 (N1 = 1.47, N3 = 0.25).

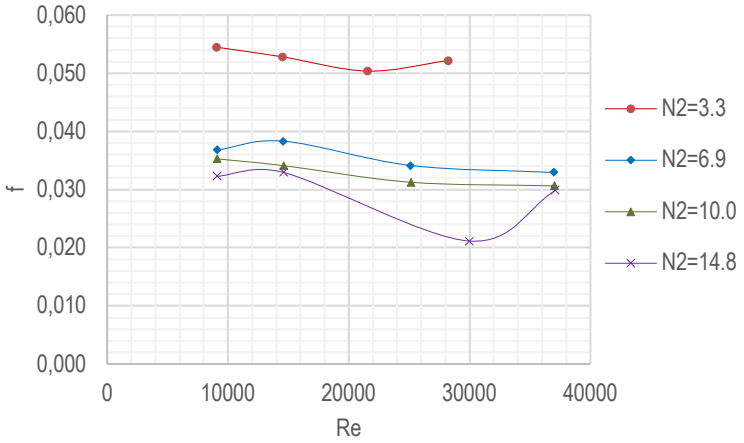

Values of the Fanning friction factor for CFD and experimental data for pipes 1 are considerably different, CFD values are around two times the experimental ones. This is because pipes 1 data sets are the ones which presented more deviations between CFD and experimental pressure drop results, also around two times greater.

The following charts are made from experimental data for the rest of the pipes and they permit to find f values for different flows and pipe geometrics.

Chart 5.13. Experimental f values in front of Re for pipes 2 (N1 = 1.73, N3 = 0.34).

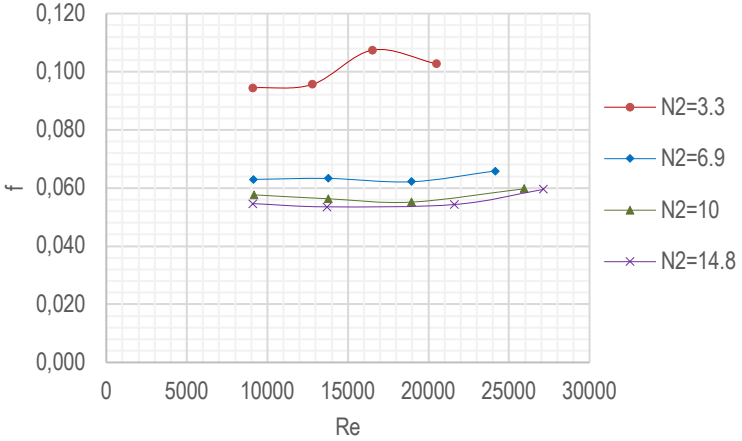

Chart 5.14. Experimental f values in front of Re for pipes 3 (N1 = 1.71, N3 = 0.29).

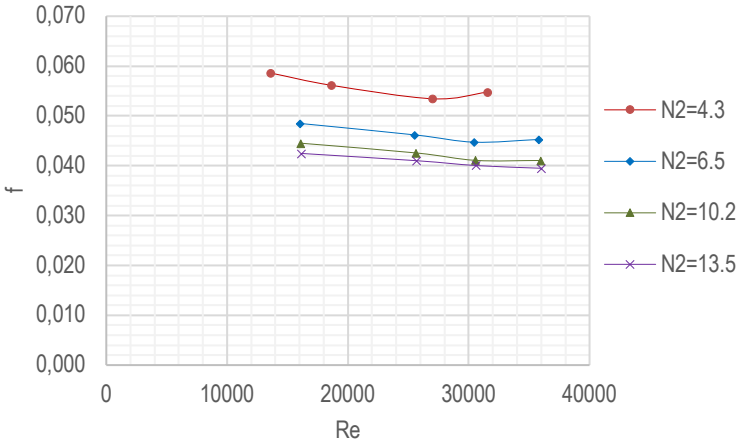

Chart 5.15. Experimental f values in front of Re for pipes 4 (N1 = 1.97, N3 = 0.23).

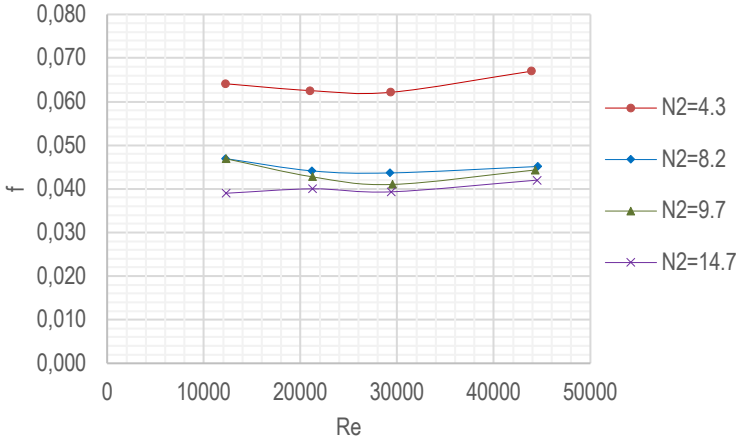

Chart 5.16. Experimental f values in front of Re for pipes 5 (N1 = 1.69, N3 = 0.22).

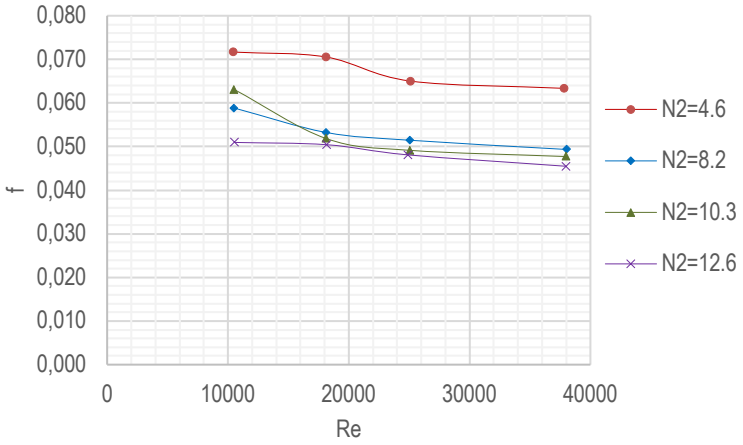

Chart 5.17. Experimental f values in front of Re for pipes 6 (N1 = 1.71, N3 = 0.20).

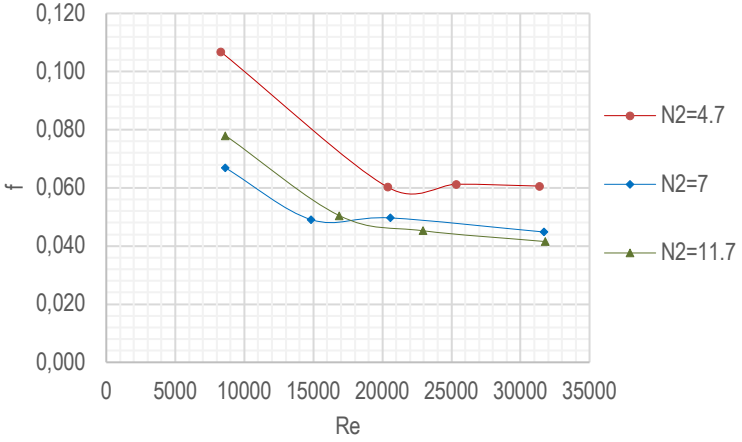

Chart 5.18. Experimental f values in front of Re for pipes 7 (N1 = 1.97, N3 = 0.23).

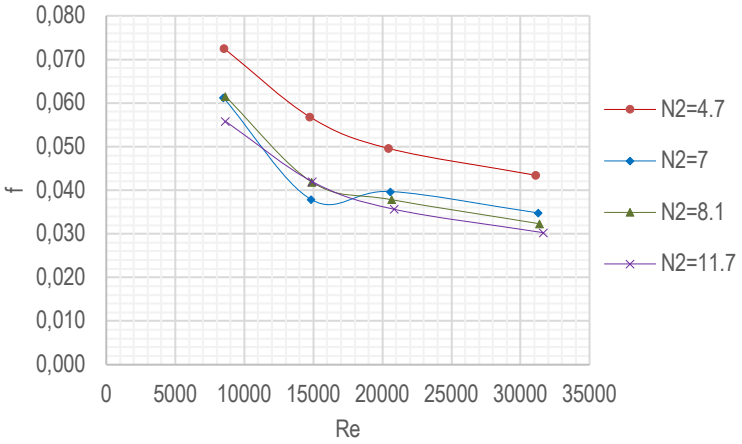

5.4. **THERMAL PERFORMANCE FACTOR**

Thermal performance factor has been calculated in order to see the effectiveness of the modifications by comparing the heat transfer enhancement and the pressure drop.

5.4.1. Smooth cylindrical pipe

Equation 1.4 uses Nu and f of a smooth cylindrical pipe without any insert as reference values. The Nusselt number have been calculated with two different equations 5.6 and 5.7 appearing in Perry's handbook were used and the value obtained were similar. Equation 5.6 (Perry, Green, & Maloney, 1992) has been chosen, because not all data sets match all criteria for equation 5.7 (Green & Southard, n.d.)

$$Nu = \frac{0.021\, Re^{0.8}\, Pr^{0.4}}{(T_w/T_m)^{0.29+0.0019\, L/D}} \tag{5.6}$$

Equation 5.6 can be used for gases when 10 < L/d < 240, 110 K < T_m < 1560 K, 1.1 < T_w/T_m < 8 and fluid properties at Tm. All data sets match these requirements, since L/d takes values from 23 to 53, the temperature of the fluid goes from 19 ºC to 100 ºC, and T_w/T_m is between 2.0 and 3.1.

$$Nu = \frac{(f/2)(Re-1000)Pr}{1+12.7\,(f/2)^{1/2}\,(Pr^{2/3}-1)}\; K \text{ where } f = 0.25\,(0.79\ln Re - 1.64)^{-2} \tag{5.7}$$

For gases, K = $(T_m/T_w)^{0.45}$ and it is valid when 0.5 < Pr < 10^5, 2300 < Re < 10^6 and 0.5 < T_m/T_w < 1.5. In this case, not all data sets also match the requirements, Pr = 0.51, Re takes values from 8752 to 45807 and T_m/T_w is between 0.3 and 0.5.

When solving this equations, an iterative method has been used, because outlet temperature, which depends on the individual heat transfer coefficient, changes T_m.

For estimating the Fanning friction factor, equation 5.8 (Levenspiel, 1993), which can be used for completely turbulent flow, and considering a surface roughness of $3 \cdot 10^{-6}$ m for the Teflon (The Engineering ToolBox, n.d.-b).

$$\frac{1}{\sqrt{f}} = 4\log\left(3.7\frac{d}{\varepsilon}\right) \tag{5.8}$$

5.4.1.1. Temperature outlet and pressure drop comparison with modified pipes

Comparing temperature outlet and pressure drop results is more visual than comparing h, Nu or f values. For this reason, the next charts 5.19 and 5.20 show the difference between the results for the modified pipes versus the calculated results for a plain pipe.

Chart 5.19. Pressure drop results comparison for every set of data.

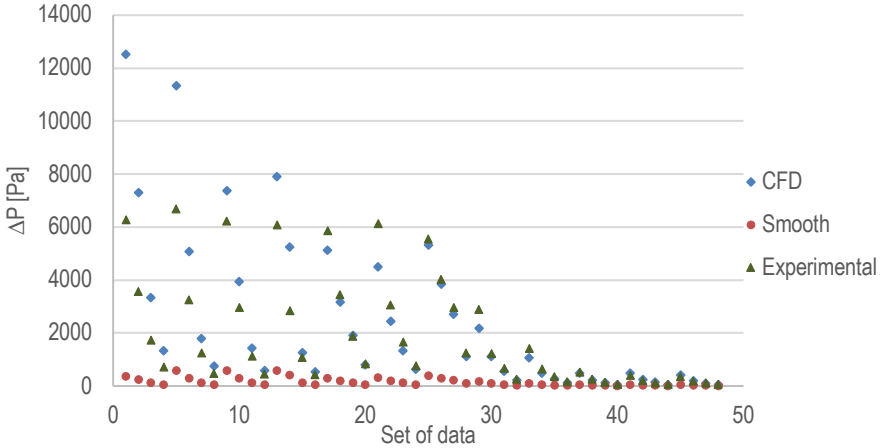

Chart 5.20. Temperature outlet results comparison for every set of data.

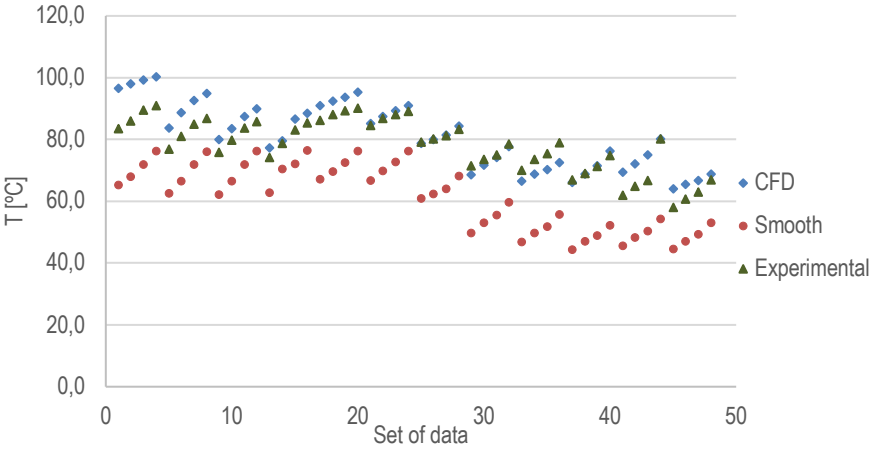

For every modified pipe, the initial data set is different, therefore a separated calculation has been done for every data set, even though there are only 5 different diameters.

Charts 5.19 and 5.20 show how both the temperature outlet and the pressure drop of the modified pipes are greater than the values obtained for a smooth cylindrical pipe without any modification. This confirms that the modifications promote heat transfer enhancement and turbulence in the flow.

The Thermal Performance Factor is only analysed for CFD results, since the same deviations commented so far also appear. In Appendix 5, there is a table with all TPF values, but what stands out is the fact all the sets of data present TPF over 1, except for sets 1D-4 and 1C-4. TPF values go from 0.95 to 3.01, with an average value of 1.32 $\pm$ 0.11. This means that heat transfer enhancement is more important than the increasing of the pressure drop, making the modified pipes perform better than a plain pipe.

5.5. **SIMULATIONS WITH DENSER MESHES**

The difficulty to get to acceptable residual values increases when N2 decreases. Pipe 1A, which has the most contorted insert did not always get to $<10^{-3}$ for continuity nor k residual values. After trying different solution methods combination, the length where the profile stabilizes was found. A new simulation with a shorter pipe and a similar number of nodes, therefore a denser mesh, was run.

The length of the pipe section was chosen after seeing Chart 21, where f and h values are represented for the length of pipe 1A1. To calculate f and h at different sections of the pipe, the temperatures of every section and the previous one have been used.

Chart 21. h and f values at different x for pipe 1A-1.

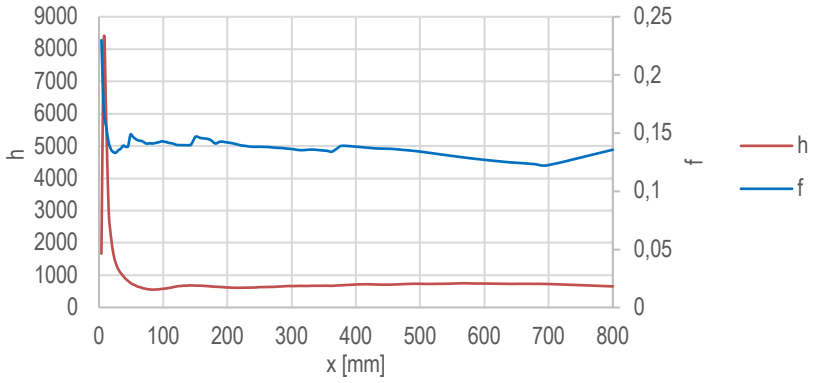

The previous graphic (5.21), shows how at the entrance of the pipe, h and f values are very high and then they stabilize. This is caused by the fact that when the fluid enters the pipe, the temperature and velocity profiles are flat, then heat and momentum transports start and the profiles evolve to the ones matching the fluid and the flow conditions.

A section of 80 crests, which represents a length of 301.8 mm was chosen to do the new mesh, which had 1.1 million nodes. When compared with the whole length of the pipe, it would be equivalent to 2.9 million nodes.

The temperature outlet al the 80th crest can be used to calculate h and f, the same way it was done for whole length pipes. Another way to get these values is taking the first 27 crests, which are 101.9 mm long, this way the highest values from the non-stabilized area are not taken into account. After that temperature outlet and pressure drop were calculated at x = 800 mm.

Table 5.5. Mesh and calculus procedure results comparison for pipe 1A.

Data set	T_{out} exp[(a)] [ºC]	ΔP exp [Pa]	T_{out} 0.8[(b)] [ºC]	ΔP 0.8 [Pa]	T_{out} 0.3[(c)] [ºC]	ΔP 0.3 [Pa]	T_{out} 0.3'[(d)] [ºC]	ΔP 0.3' [Pa]
1	83,5	6257	95,2	16263	96,7	12516	97,2	10347
2	86,0	3560	97,5	8697	98,1	7285	98,5	5812
3	89,5	1716	99,8	3883	99,4	3328	99,6	2776
4	91,0	696	101	1611	100,3	1330	100,4	1084

(a) Experimental results.
(b) CFD results of the whole pipe (0.800 m).
(c) CFD results of the 80 first crests (0.301 m).
(d) CFD results of the 80 first crests, excluding the 27 initial ones.

The obtained results appear on Table 5.5, which permits to compare the different methods used. The most important thing to mention is that all CFD obtained results are very similar, the maximum differences are 2 ºC (2% error) and 5916 Pa (36% error) between them. This confirms that the mesh used for all the data sets has no influence in the results obtained.

Even though the simulation run for the whole pipe has slightly more similar results to experimental data, in the previous subsections the values used are ones obtained from the shortened pipe with the initial crests considered. They has been chosen because the convergence was better, all the residuals were $<10^{-3}$.

6. CONCLUSIONS

The main conclusions of this project, are, in the first place, that the mesh used was dense enough not to affect the simulation results. For the studied pipes, the best turbulence model is k-ω SST, one of the most common RANS models.

Secondly, it has been concluded that CFD simulations are an acceptable method to predict the performance of this kind of pipes, due to the similarity of the obtained results with the experimental ones.

Regarding the effect of pipe geometric characteristics, it has been seen that when the twisted tape insert is more contorted, both heat transfer, and pressure drop increase. This occurs because the fluid is deflected from its axial path, causing more turbulence.

It has not been possible to thoroughly analyse the influence of the crests height and width because of the pipes characteristics. A future research would run simulations with different geometric characteristics, where the number of crests varies and the height is constant and backwards. Still, it has been observed that convective heat transfer and pressure drop increase then the size of the crests also increase, this tendency is specially clear in the heat transfer.

The Nusselt number, as expected, increases with the Reynolds number, this another proof that turbulence enhances convective heat transfer. For the Fanning friction factor, there is not any evident lineal relation with Re.

After these observations, the adjusted equations 5.5 can be used as a guide for optimization of the pipe characteristics, being very useful to set the design direction.

Finally, the TPF values allow to affirm that heat transfer enhancement is more important than pressure drop increase. The modifies pipes have a better performance than a plain pipe.

REFERENCES AND NOTES

1. Bhuiya, M. M. K., Chowdhury, M. S. U., Shahabuddin, M., Saha, M., & Memon, L. A. (2013). Thermal characteristics in a heat exchanger tube fitted with triple twisted tape inserts. International Communications in Heat and Mass Transfer, 48, 124–132. https://doi.org/10.1016/J.ICHEATMASSTRANSFER.2013.08.024
2. Bird, R. B. (Robert B., Stewart, W. E., & Lightfoot, E. N. (2002). Transport phenomena. Retrieved from http://cercabib.ub.edu/iii/encore/record/C__Rb2041023__S Transport Phenomena__P0,3__Orightresult__U__X7?lang=cat&suite=def
3. Caliskan, S. (2014). Experimental investigation of heat transfer in a channel with new winglet-type vortex generators. International Journal of Heat and Mass Transfer, 78, 604–614. https://doi.org/10.1016/J.IJHEATMASSTRANSFER.2014.07.043
4. Chamarro Aguilera, M. E. (1988). Tubos para intercambiadores de calor gas-gas de alto rendimiento. Universitat de Barcelona.
5. Date, A. W. (Anil W. (2009). Introduction to computational fluid dynamics. Retrieved from https://www.mendeley.com/import/?url=http://cercabib.ub.edu/iii/encore/record/C__Rb2170449__Sintroduction to computational fluid dynamics__Orightresult__U__X7?lang=cat&suite=def
6. Eiamsa-ard, S., Thianpong, C., & Eiamsa-ard, P. (2010). Turbulent heat transfer enhancement by counter/co-swirling flow in a tube fitted with twin twisted tapes. Experimental Thermal and Fluid Science, 34(1), 53–62. https://doi.org/10.1016/J.EXPTHERMFLUSCI.2009.09.002
7. EIAMSA-ARD, S., & WONGCHAREE, K. (2013). Heat transfer characteristics in micro-fin tube equipped with double twisted tapes: Effect of twisted tape and micro-fin tube arrangements. Journal of Hydrodynamics, Ser. B, 25(2), 205–214. https://doi.org/10.1016/S1001-6058(13)60355-8
8. Eiamsa-ard, S, Nanan, K., Thianpong, C., & Eiamsa-ard, P. (2013). Thermal Performance Evaluation of Heat Exchanger Tubes Equipped with Coupling Twisted Tapes. Experimental Heat Transfer, 26(5), 413–430. https://doi.org/10.1080/08916152.2012.704483
9. Eiamsa-ard, Smith, Nuntadusit, C., & Promvonge, P. (2013). Effect of Twin Delta-Winged Twisted-Tape on Thermal Performance of Heat Exchanger Tube. Heat Transfer Engineering, 34(15), 1278–1288. https://doi.org/10.1080/01457632.2013.793112
10. Eiamsa-ard, Smith, & Promvonge, P. (2010a). Performance assessment in a heat exchanger tube with alternate clockwise and counter-clockwise twisted-tape inserts. International Journal of Heat and Mass Transfer, 53(7–8), 1364–1372. https://doi.org/10.1016/J.IJHEATMASSTRANSFER.2009.12.023
11. Eiamsa-ard, Smith, & Promvonge, P. (2010b). Thermal characteristics in round tube fitted with serrated twisted tape. Applied Thermal Engineering, 30(13), 1673–1682. https://doi.org/10.1016/J.APPLTHERMALENG.2010.03.026
12. Eiamsa-ard, Smith, Thianpong, C., Eiamsa-ard, P., & Promvonge, P. (2009). Convective heat transfer in a circular tube with short-length twisted tape insert. International Communications in Heat and Mass Transfer, 36(4), 365–371. https://doi.org/10.1016/j.icheatmasstransfer.2009.01.006
13. Esmaeilzadeh, E., Almohammadi, H., Nokhosteen, A., Motezaker, A., & Omrani, A. N. (2014). Study on heat transfer and friction factor characteristics of γ-Al2O3/water through circular tube

with twisted tape inserts with different thicknesses. International Journal of Thermal Sciences, 82(1), 72–83. https://doi.org/10.1016/j.ijthermalsci.2014.03.005
14. Gawande, V., Dhoble, A., & Zodpe, D. B. (2015). Experimental and CFD-based thermal performance prediction of solar air heater provided with chamfered square rib as artificial roughness. In J. Braz. Soc. Mech. Sci. Eng.
15. Green, D. W., & Southard, M. Z. (n.d.). Perry's chemical engineers' handbook. Retrieved from https://www.accessengineeringlibrary.com/browse/perrys-chemical-engineers-handbook-9th-edition
16. Hasanpour, A., Farhadi, M., & Sedighi, K. (2014). A review study on twisted tape inserts on turbulent flow heat exchangers: The overall enhancement ratio criteria. International Communications in Heat and Mass Transfer, 55, 53–62. https://doi.org/10.1016/j.icheatmasstransfer.2014.04.008
17. Jaisankar, S., Radhakrishnan, T. K., & Sheeba, K. N. (2009). Experimental studies on heat transfer and friction factor characteristics of forced circulation solar water heater system fitted with helical twisted tapes. Solar Energy, 83(11), 1943–1952. https://doi.org/10.1016/J.SOLENER.2009.07.006
18. Khoshvaght-Aliabadi, M., Tavasoli, M., & Hormozi, F. (2015). Comparative analysis on thermal–hydraulic performance of curved tubes: Different geometrical parameters and working fluids. Energy, 91, 588–600. https://doi.org/10.1016/J.ENERGY.2015.08.088
19. Khoshvaght-Aliabadi, Morteza, & Arani-Lahtari, Z. (2016). Forced convection in twisted minichannel (TMC) with different cross section shapes: A numerical study. Applied Thermal Engineering, 93, 101–112. https://doi.org/10.1016/J.APPLTHERMALENG.2015.09.010
20. Kumar, S., & Amano, R. S. (2015). Experimental investigation of heat transfer and flow using V and broken V ribs within gas turbine blade cooling passage. Heat and Mass Transfer, 51(5), 631–647. https://doi.org/10.1007/s00231-014-1436-8
21. Léal, L., Miscevic, M., Lavieille, P., Amokrane, M., Pigache, F., Topin, F., … Tadrist, L. (2013). An overview of heat transfer enhancement methods and new perspectives: Focus on active methods using electroactive materials. International Journal of Heat and Mass Transfer, 61(1), 505–524. https://doi.org/10.1016/j.ijheatmasstransfer.2013.01.083
22. Levenspiel, O. (1993). Flujo de fluidos e intercambio de calor. Retrieved from http://cercabib.ub.edu/iii/encore/record/C__Rb1987826__Sengineering flow and heat exchange__Orightresult__U__X3?lang=cat&suite=def
23. Lotfi, B., Sundén, B., & Wang, Q. (2016). An investigation of the thermo-hydraulic performance of the smooth wavy fin-and-elliptical tube heat exchangers utilizing new type vortex generators. Applied Energy, 162, 1282–1302. https://doi.org/10.1016/j.apenergy.2015.07.065
24. Maradiya, C., Vadher, J., & Agarwal, R. (2017). The heat transfer enhancement techniques and their Thermal Performance Factor. Beni-Suef University Journal of Basic and Applied Sciences, 7(1), 1–21. https://doi.org/10.1016/j.bjbas.2017.10.001
25. McDonough, J. M. (2007). Introductory Lectures on Turbulence, Physics, Mathematics and Modeling. Departments of Mechanical Engineering and Mathematics University of Kentucky.
26. Menter Florian. (2019). Best Practice : Generalized k- w Two-Equation Turbulence Model in ANSYS CFD (GEKO). 1–38.
27. Murugesan, P., Mayilsamy, K., & Suresh, S. (2010). Turbulent Heat Transfer and Pressure Drop in Tube Fitted with Square-cut Twisted Tape. Chinese Journal of Chemical Engineering, 18(4), 609–617. https://doi.org/10.1016/S1004-9541(10)60264-9
28. Perry, R. H., Green, D. W., & Maloney, J. O. (1992). Perry : manual del ingeniero químico. Retrieved from http://cercabib.ub.edu/iii/encore/record/C__Rb1192345__SPerry__Orightresult__U__X6?lang=cat&suite=def
29. Petkov, V. M., Zimparov, V. D., & Bergles, A. E. (2014). Performance evaluation of ducts with non-circular shapes: Laminar fully developed flow and constant wall temperature. International Journal of Thermal Sciences, 79, 220–228.

https://doi.org/10.1016/J.IJTHERMALSCI.2013.12.005
30. Promvonge, P. (2008). Thermal augmentation in circular tube with twisted tape and wire coil turbulators. Energy Conversion and Management, 49(11), 2949–2955. https://doi.org/10.1016/J.ENCONMAN.2008.06.022
31. Promvonge, P., Suwannapan, S., Pimsarn, M., & Thianpong, C. (2014). Experimental study on heat transfer in square duct with combined twisted-tape and winglet vortex generators. International Communications in Heat and Mass Transfer, 59, 158–165. https://doi.org/10.1016/J.ICHEATMASSTRANSFER.2014.10.005
32. Rahimi, M., Shabanian, S. R., & Alsairafi, A. A. (2009). Experimental and CFD studies on heat transfer and friction factor characteristics of a tube equipped with modified twisted tape inserts. Chemical Engineering and Processing: Process Intensification, 48(3), 762–770. https://doi.org/10.1016/J.CEP.2008.09.007
33. Rao, Y., Li, B., & Feng, Y. (2015). Heat transfer of turbulent flow over surfaces with spherical dimples and teardrop dimples. Experimental Thermal and Fluid Science, 61, 201–209. https://doi.org/10.1016/J.EXPTHERMFLUSCI.2014.10.030
34. Sadrehaghighi, I. (2019). Turbulence Modeling -A review. (November). https://doi.org/10.13140/RG.2.2.35857.33129/2
35. Salam, B., Biswas, S., Saha, S., & Bhuiya, M. M. K. (2013). Heat Transfer Enhancement in a Tube using Rectangular-cut Twisted Tape Insert. Procedia Engineering, 56, 96–103. https://doi.org/10.1016/J.PROENG.2013.03.094
36. Salameh, T., Alami, A. H., & Sunden, B. (2016). Experimental investigation of the effect of variously-shaped ribs on local heat transfer on the outer wall of the turning portion of a U-channel inside solar air heater. Heat and Mass Transfer, 52(3), 539–546. https://doi.org/10.1007/s00231-015-1541-3
37. Sarada, S. N., Raju, A. S. R., Radha, K. K., & Sunder, L. S. (2011). Enhancement of heat transfer using varying width twisted tape inserts. International Journal of Engineering, Science and Technology, 2(6), 107–118. https://doi.org/10.4314/ijest.v2i6.63702
38. Shabanian, S. R., Rahimi, M., Shahhosseini, M., & Alsairafi, A. A. (2011). CFD and experimental studies on heat transfer enhancement in an air cooler equipped with different tube inserts. International Communications in Heat and Mass Transfer, 38(3), 383–390. https://doi.org/10.1016/j.icheatmasstransfer.2010.12.015
39. Skullong, S., Promvonge, P., Thianpong, C., & Pimsarn, M. (2016). Heat transfer and turbulent flow friction in a round tube with staggered-winglet perforated-tapes. International Journal of Heat and Mass Transfer, 95, 230–242. https://doi.org/10.1016/J.IJHEATMASSTRANSFER.2015.12.007
40. Tang, X., Dai, X., & Zhu, D. (2015). Experimental and numerical investigation of convective heat transfer and fluid flow in twisted spiral tube. International Journal of Heat and Mass Transfer, 90, 523–541. https://doi.org/10.1016/j.ijheatmasstransfer.2015.06.068
41. The Engineering ToolBox. (n.d.-a). Engineering ToolBox. Retrieved March 21, 2019, from https://www.engineeringtoolbox.com/
42. The Engineering ToolBox. (n.d.-b). Lined Pipes and Pressure Drop. Retrieved May 25, 2019, from https://www.engineeringtoolbox.com/lined-pipe-pressure-loss-d_1178.html
43. The Engineering ToolBox. (n.d.-c). Polymers - Physical Properties. Retrieved April 4, 2019, from https://www.engineeringtoolbox.com/polymer-properties-d_1222.html
44. Thianpong, C., Eiamsa-ard, P., Promvonge, P., & Eiamsa-ard, S. (2012). Effect of perforated twisted-tapes with parallel wings on heat tansfer enhancement in a heat exchanger tube. Energy Procedia, 14, 1117–1123. https://doi.org/10.1016/J.EGYPRO.2011.12.1064
45. Vashistha, C., Patil, A. K., & Kumar, M. (2016). Experimental investigation of heat transfer and pressure drop in a circular tube with multiple inserts. Applied Thermal Engineering, 96, 117–129. https://doi.org/10.1016/j.applthermaleng.2015.11.077

46. Wongcharee, K., & Eiamsa-ard, S. (2011). Heat transfer enhancement by twisted tapes with alternate-axes and triangular, rectangular and trapezoidal wings. Chemical Engineering and Processing: Process Intensification, 50(2), 211–219. https://doi.org/10.1016/J.CEP.2010.11.012
47. Yadav, A. S., & Bhagoria, J. L. (2014). A CFD based thermo-hydraulic performance analysis of an artificially roughened solar air heater having equilateral triangular sectioned rib roughness on the absorber plate. International Journal of Heat and Mass Transfer, 70, 1016–1039. https://doi.org/10.1016/J.IJHEATMASSTRANSFER.2013.11.074
48. Zdanski, P. S. B., Pauli, D., & Dauner, F. A. L. (2015). Effects of delta winglet vortex generators on flow of air over in-line tube bank: A new empirical correlation for heat transfer prediction. International Communications in Heat and Mass Transfer, 67, 89–96. https://doi.org/10.1016/j.icheatmasstransfer.2015.07.010
49. Zhai, C., Islam, M. D., Alam, M. M., Simmons, R., & Barsoum, I. (2019). Parametric study of major factors affecting heat transfer enhancement in a circular tube with vortex generator pairs. Applied Thermal Engineering, 153(March), 330–340. https://doi.org/10.1016/j.applthermaleng.2019.03.018
50. Zhang, C., Wang, D., Ren, K., Han, Y., Zhu, Y., & Peng, X. (2016). A comparative review of self-rotating and stationary twisted tape inserts in heat exchanger. Renewable and Sustainable Energy Reviews, 53, 433–449. https://doi.org/10.1016/j.rser.2015.08.048
51. Zhu, X. W., Fu, Y. H., & Zhao, J. Q. (2016). A novel wavy-tape insert configuration for pipe heat transfer augmentation. Energy Conversion and Management, 127(4), 140–148. https://doi.org/10.1016/j.enconman.2016.09.006

ACRONYMS

A	heat transfer surface area
C	distance between two crest pics
CFD	Computerized Fluid Dynamics
CI	confidence interval
Cp	specific heat
D, d	diameter
Dh	hydraulic diameter
DNS	Direct Numerical Simulation
f	Fanning friction factor
g	gravity
h	individual heat transfer coefficient
H	length of a 180º turn
k	thermal conductivity
l	length
L	pipe length
LES	Large-Eddy Simulation
N	Number of crests
N1	D/d
N2	H/d
N3	C/d
Nu	Nusselt number
P, p	pressure
Pr	Prandtl number
$\vec{q}$	heat flow through a unit area
Q	heat flow
R	correlation coefficient
RANS	Reynolds Average Navier-Stokes
Re	Reynolds number
RSS	Sum of Squares due to Regression
T	temperature
t	time
TPF	Thermal Performance Factor
tt	twisted tape
ttW	twisted tape width
U	global heat transfer coefficient
u, U	velocity vector
v	mean velocity
μ	viscosity
ρ	density

Subscripts and accents

0	smooth pipe reference
eff	effective
f	fluid
lm	logarithmic mean
m	mean
ref	reference
s	solid
t	turbulent
w	wall
$\bar{}$	time averaged

APPENDICES

APPENDIX 1: SUMMARY OF HEAT TRANSFER ENHANCEMENT TECHNIQUES

Table A1.1. Heat enhancement techniques and their TPF.

Reference	Modification	Re	Fluid	TPF
Eiamsa-ard et al., 2009	Short length tt	5000 10000 20000	Air	0.98 0.95 0.91
Eiamsa-ard & Promvonge, 2010a	Alternate clockwise and counter-clockwise	5000 10000 20000	Water	1.35 1.26 1.18
Rahimi et al., 2009	Jagged tt	5000 10000	Water	1.17 1.09
Shabanian et al., 2011	Butterfly tt	5000 10000	Water	1.60 1.53
Eiamsa-ard et al., 2013	Twin Delta winglet tape	5000 10000	Water	1.24 1.12
Eiamsa-ard & Promvonge, 2010a	Delta winglet tt	5000 10000 20000	Water	1.22 1.18 1.15
Promvonge et al., 2014	Tt with winglet VG	5000 10000 20000	Air	1.56 1.48 1.38
Wongcharee & Eiamsa-ard, 2011	Tt with alternate axes and triangular wing	5000 10000 20000	Water	1.42 1.25 1.13
Eiamsa-ard & Wongcharee, 2013	Counter double tt	5000 10000 20000	Water	2.02 1.76 1.50
Bhuiya et al., 2013	Triple tt	5000 10000 20000	Air	1.44 1.40 1.33
Skullong et al., 2016	Staggered winglet perforated tape	5000 10000 20000	Air	1.7 1.58 1.48

Yadav & Bhagoria, 2014	Triangular sectioned rib as roughness on absorber plate	5000 10000 20000	Air	2.05 2.07 1.98
Gawande et al., 2015	Right α triangular rib as roughness on absorber surface	5000 10000 20000	Air	1.99 2.01 1.98
Rao, Li, & Feng, 2015	Surfaces with spherical and tear drop dimples	5000 10000 20000	Air	1.48 1.51 1.53
Salameh et al., 2016	Perforated rib	5000 10000 20000	Air	2.8 2.45 1.9
Caliskan, 2014	Punched triangular VG	5000 10000 20000	Air	2.7 2.48 2.2
Tang et al., 2015	Twisted tri-lobed inner tube	10000 20000	Water	1.11 1.04
Jaisankar et al., 2009	Typical tt	3000-23000		1-1.2
Eiamsa-ard et al., 2010	Twin counter tt	4000-19000		1.4
Thianpong et al., 2012	Perforated tt	5500 & 20500		1.32
Eiamsa-ard & Promvonge, 2010b	Serrated tt	4000-20000		1.2
Salam et al., 2013	Square cut tt	10000-19000		1.9
Murugesan et al., 2010	Square cut tt	2000-12000		1.06-1.2
Promvonge, 2008	Wire coiled and tt inserts	3000-18000		1.6
Zhu, Ru, & Zhao, 2016	Wavy-tape insert	200 2200		1.70 1.82

APPENDIX 2: SETUP EXPLORATION RESULT

Chart A2.1. Model exploration results, set of data 4A-1.

Model	T_{out} **exp** [°C]	Δ**P exp** [Pa]	T_{out} [°C]	Δ**P** [Pa]
k-ω Standad	78.5	4237	84.5	4556
k-ω SST	78.5	4237	82.8	4024
k-ω GEKO	78.5	4237	86.3	4858
k-ω BSL	78.5	4237	84.8	5016
k-kl-ω	78.5	4237	91.6	6623
Transition SST	78.5	4237	84.8	4544
k-ε	78.5	4237	87.7	6545

Chart A2.2. Teflon thickness exploration results, set of data 4A-1.

Thickness [mm]	T_{out} **exp** [°C]	Δ**P exp** [Pa]	T_{out} [°C]	Δ**P** [Pa]
0.35	78.5	4237	82.5	3841
0.40	78.5	4237	83.6	4157
0.50	78.5	4237	82.8	4024

Chart A2.3. Mesh exploration results, set of data 4B-2.

Number of nodes	**Element size** [m]	**Growth Rate**	T_{out} **exp** [°C]	Δ**P exp** [Pa]	T_{out} [°C]	Δ**P** [Pa]
23338	$6 \cdot 10^{-3}$	1.5	73.5	1216	78.4	2011
739365	$1 \cdot 10^{-3}$	2.0	73.5	1216	73.0	1078
760371	$1 \cdot 10^{-3}$	1.7	73.5	1216	73.0	1050
870970	$5 \cdot 10^{-3}$	1.2	73.5	1216	73.0	1095
1389513	$8 \cdot 10^{-4}$	1.5	73.5	1216	72.0	1018
2583719	$6 \cdot 10^{-4}$	1.7	73.5	1216	71.8	890

APPENDIX 3: RESULTS

Set of data	N1	N2	N3	T_{in} [ºC]	T_{out} [ºC]	T_w [ºC]	ΔP [Pa]	v_{in} [m/s]	ρ_{in} [kg/m³]	ΔT_{lm} [ºC]	T_m [ºC]	Re	U·A [J/(s ºC)]	h [J/(s m² ºC)]	Nu	Pr	f
1A-1	1.47	3.3	0.25	19.7	96.5	102.2	12516	30.528	1.206	28.8	58.1	27814	11.69	775	406	0.51	0.104
1A-2	1.47	3.3	0.25	20.5	97.9	102.0	7285	23.468	1.203	25.8	59.2	21273	9.97	542	283	0.51	0.103
1A-3	1.47	3.3	0.25	21.5	99.3	101.9	3328	15.937	1.199	22.8	60.4	14361	7.48	322	168	0.51	0.102
1A-4	1.47	3.3	0.25	22.8	100.2	102.0	1330	10.019	1.193	20.4	61.5	8960	4.99	178	93	0.51	0.104
1B-1	1.47	6.9	0.25	19.6	83.7	102.4	11320	39.673	1.206	43.0	51.7	36683	8.59	408	217	0.51	0.056
1B-2	1.47	6.9	0.25	20.2	88.7	102.1	5066	27.166	1.204	37.9	54.4	24918	6.73	273	144	0.51	0.053
1B-3	1.47	6.9	0.25	21.3	92.6	102.0	1772	15.937	1.199	33.1	57.0	14473	4.54	157	83	0.51	0.055
1B-4	1.47	6.9	0.25	22.4	94.9	102.0	744	10.019	1.195	30.0	58.7	9033	3.16	100	52	0.51	0.058
1C-1	1.47	10.0	0.25	19.4	79.9	102.0	7362	39.673	1.207	45.9	49.6	36888	6.77	276	148	0.51	0.036
1C-2	1.47	10.0	0.25	20.2	83.5	102.1	3921	27.166	1.204	42.7	51.9	25066	5.41	199	106	0.51	0.041
1C-3	1.47	10.0	0.25	21.4	87.4	102.1	1421	15.937	1.199	38.8	54.4	14559	3.58	116	61	0.51	0.044
1C-4	1.47	10.0	0.25	22.7	89.9	101.9	561	10.019	1.194	35.7	56.3	9075	2.45	74	39	0.51	0.044
1D-1	1.47	14.8	0.25	19.9	77.2	102.5	7890	39.741	1.205	48.4	48.6	36980	6.61	266	143	0.51	0.039
1D-2	1.47	14.8	0.25	20.6	79.7	102.4	5233	32.378	1.202	46.1	50.1	29948	5.74	216	115	0.51	0.039
1D-3	1.47	14.8	0.25	21.7	86.7	102.2	1246	15.937	1.198	39.5	54.2	14551	3.40	109	58	0.51	0.038
1D-4	1.47	14.8	0.25	23.2	88.5	102.1	526	10.019	1.192	37.1	55.9	9068	2.29	69	36	0.51	0.041
2B-1	1.73	6.9	0.34	21.0	90.9	102.0	5109	26.359	1.201	35.2	56.0	24033	7.16	301	158	0.51	0.057
2B-2	1.73	6.9	0.34	21.7	92.3	101.8	3159	20.788	1.198	33.1	57.0	18861	5.93	226	119	0.51	0.057
2B-3	1.73	6.9	0.34	22.5	93.7	101.5	1894	15.197	1.195	30.7	58.1	13719	4.89	173	91	0.51	0.064
2B-4	1.73	6.9	0.34	23.6	95.3	101.6	784	10.154	1.190	28.6	59.4	9101	3.28	105	55	0.51	0.060
2C-1	1.73	10.0	0.34	21.2	85.2	102.1	4484	28.309	1.200	40.9	53.2	25953	6.02	231	123	0.51	0.044

Set of data	N1	N2	N3	T_{in} [ºC]	T_{out} [ºC]	T_w [ºC]	ΔP [Pa]	v_{in} [m/s]	ρ_{in} [kg/m^3]	ΔT_{lm} [ºC]	T_m [ºC]	Re	U·A [J/(s ºC)]	h [J/(s m^2 ºC)]	Nu	Pr	f
2C-2	1.73	10.0	0.34	21.8	87.5	102.0	2422	20.778	1.197	38.4	54.7	18938	4.72	165	87	0.51	0.044
2C-3	1.73	10.0	0.34	22.5	89.2	101.9	1333	15.197	1.195	36.4	55.9	13790	3.65	119	63	0.51	0.045
2C-4	1.73	10.0	0.34	23.5	90.9	101.7	627	10.154	1.191	34.1	57.2	9155	2.60	80	42	0.51	0.048
3C-1	1.71	10.2	0.29	22.9	78.6	102.1	5315	34.670	1.193	45.8	50.8	36015	7.52	268	162	0.51	0.039
3C-2	1.71	10.2	0.29	23.1	80.0	101.9	3827	29.541	1.192	44.4	51.6	30605	6.65	223	135	0.51	0.039
3C-3	1.71	10.2	0.29	23.3	81.4	102.0	2707	24.823	1.192	43.4	52.3	25671	5.78	183	111	0.51	0.039
3C-4	1.71	10.2	0.29	24.1	84.4	101.8	1114	15.694	1.188	40.3	54.3	16104	4.01	115	69	0.51	0.040
4B-1	1.48	8.6	0.18	22.9	68.5	101.7	2177	28.925	1.193	52.7	45.7	44711	9.84	226	204	0.51	0.034
4B-2	1.48	8.6	0.18	23.7	71.7	101.4	1099	19.125	1.190	49.9	47.7	29351	7.38	153	137	0.51	0.039
4B-3	1.48	8.6	0.18	24.2	74.2	101.4	554	13.887	1.188	47.9	49.2	21202	5.64	109	97	0.51	0.038
4B-4	1.48	8.6	0.18	25.3	77.7	101.4	202	8.129	1.184	44.9	55.5	12303	3.63	65	58	0.51	0.040
5C-1	1.69	10.3	0.22	21.3	66.5	102.2	1045	21.075	1.199	55.2	43.9	38141	9.20	168	177	0.51	0.036
5C-2	1.69	10.3	0.22	21.9	68.9	102.1	475	14.011	1.197	53.3	45.4	25227	6.55	109	114	0.51	0.037
5C-3	1.69	10.3	0.22	22.2	70.2	101.8	257	10.157	1.196	52.0	46.2	18237	4.95	78	82	0.51	0.038
5C-4	1.69	10.3	0.22	23.5	72.5	101.7	102	5.955	1.191	49.8	48.0	10604	3.08	46	48	0.51	0.044
6B-1	1.71	7.0	0.20	22.0	66.1	101.0	467	14.562	1.197	54.0	44.0	31745	9.29	133	169	0.51	0.040
6B-2	1.71	7.0	0.20	22.6	68.8	100.9	211	9.507	1.194	51.8	45.7	20592	6.61	88	111	0.51	0.043
6B-3	1.71	7.0	0.20	23.0	71.4	100.9	122	6.890	1.193	49.8	47.2	14858	5.21	67	84	0.51	0.047
6B-4	1.71	7.0	0.20	23.8	76.3	100.9	46	4.026	1.190	46.0	50.0	8603	3.58	44	55	0.51	0.052
7B-1	1.97	7.0	0.23	23.3	69.4	101.7	485	14.383	1.192	52.0	46.4	31052	9.96	146	184	0.51	0.043
7B-2	1.97	7.0	0.23	24.0	72.1	101.7	222	9.529	1.189	49.9	48.0	20441	7.12	96	121	0.51	0.045

Set of data	N1	N2	N3	T_{in} [ºC]	T_{out} [ºC]	T_w [ºC]	ΔP [Pa]	v_{in} [m/s]	ρ_{in} [kg/m^3]	ΔT_{lm} [ºC]	T_m [ºC]	Re	U·A [J/(s ºC)]	h [J/(s m^2 ºC)]	Nu	Pr	f
7B-3	1.97	7.0	0.23	24.8	75.0	101.5	127	6.912	1.186	47.3	49.9	14726	5.67	74	92	0.51	0.049
7B-4	1.97	7.0	0.23	26.8	80.1	101.4	50	4.049	1.178	42.5	53.5	8498	3.90	49	60	0.51	0.057
7D-1	1.97	11.7	0.23	21.8	63.9	101.9	411	14.394	1.197	56.4	42.9	31465	8.41	118	150	0.51	0.036
7D-2	1.97	11.7	0.23	22.6	65.5	101.6	185	9.540	1.194	54.8	44.0	20745	5.81	76	96	0.51	0.037
7D-3	1.97	11.7	0.23	23.5	66.8	101.4	99	6.878	1.191	53.4	45.1	14880	4.33	54	69	0.51	0.038
7D-4	1.97	11.7	0.23	24.8	68.8	101.5	35	4.026	1.186	51.6	46.8	8639	2.65	32	40	0.51	0040

APPENDIX 4: ADDITIONAL CHARTS

Chart A3.1. Nu values in front of Reynolds for pipes 1 & 2 B (N2 = 6.9).

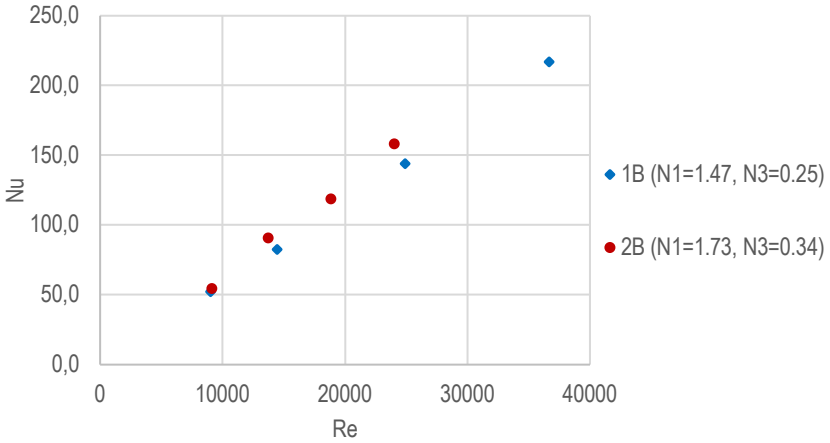

Chart A3.2. Nu values in front of Reynolds for pipes 1 & 2 C (N2=10.0).

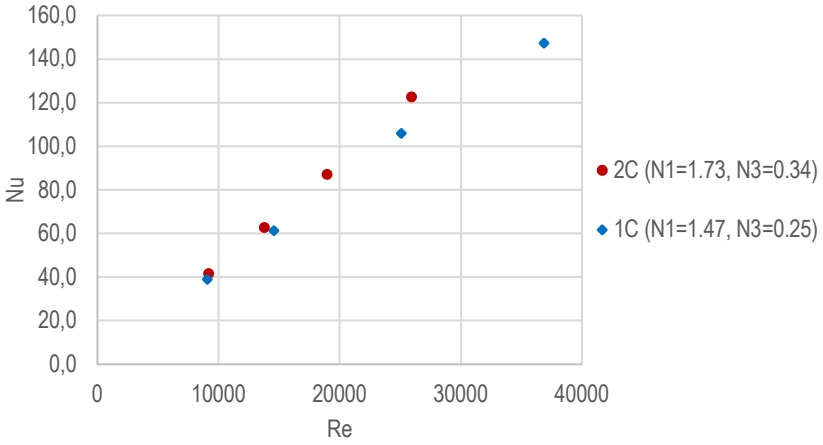

Chart A3.3. f values in front of Reynolds for pipes 1 & 2 B (N2=6.9).

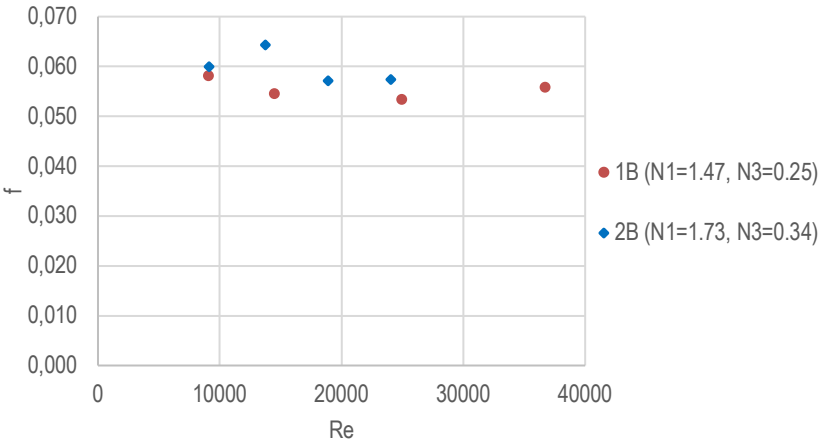

Chart A3.3. f values in front of Reynolds for pipes 6 & 7 B (N2=7.0).

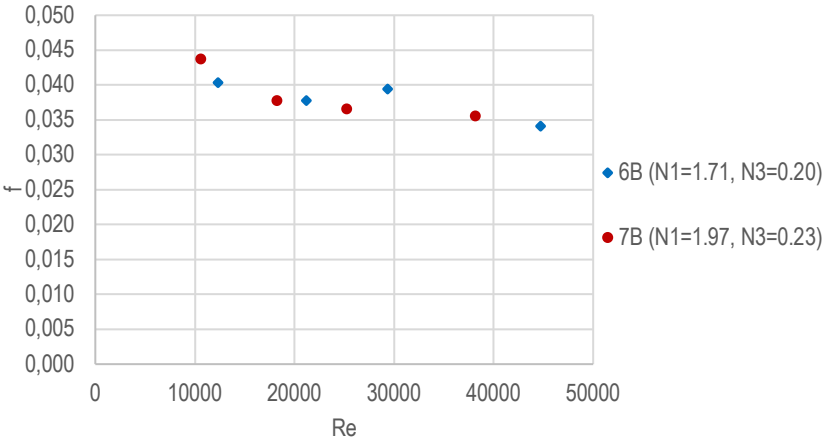

APPENDIX 5: THERMAL PERFORMANCE FACTOR

In the following table, temperatures are in ºC, the pressure drop in Pa, and h in J/(s m ºC).

Data set	Re	$Nu^{(a)}$	$h^{(a)}$	$T_{out}^{(a)}$	$f^{(b)}$	$Nu^{(b)}$	$h^{(b)}$	$T_{out}^{(b)}$	f	ΔP	TPF	TPF_{exp}
1A-1	28844	55	101	65.2	0.006	52	95	63.7	0.0060	360	3.01	1.12
1A-2	22024	45	82	68.0	0.006	43	79	66.8	0.0064	226	2.63	1.11
1A-3	14821	33	61	71.9	0.007	32	59	71.2	0.0070	114	2.16	1.09
1A-4	9210	22	42	76.3	0.008	22	41	76.0	0.0080	51	1.77	0.98
1B-1	37607	68	125	62.5	0.006	64	116	60.8	0.0057	575	1.59	1.11
1B-2	25569	50	92	66.5	0.006	48	88	65.1	0.0062	293	1.47	1.07
1B-3	14825	33	61	71.9	0.007	32	59	71.2	0.0070	114	1.31	0.97
1B-4	9231	22	42	76.1	0.008	22	41	75.8	0.0080	51	1.21	0.92
1C-1	37662	68	125	62.2	0.006	64	116	60.5	0.0057	575	1.25	1.10
1C-2	25569	50	92	66.5	0.006	48	88	65.1	0.0062	293	1.18	1.05
1C-3	14821	33	61	72.0	0.007	32	59	71.3	0.0070	114	1.05	0.95
1C-4	9220	22	42	76.2	0.008	22	41	75.9	0.0080	51	1.00	0.89
1D-1	37615	68	125	62.7	0.006	64	116	61.0	0.0057	576	1.18	1.01
1D-2	30274	58	107	70.4	0.006	54	100	68.8	0.0060	400	1.14	0.98
1D-3	14798	33	60	72.2	0.007	32	59	71.5	0.0070	114	1.03	0.93
1D-4	9195	22	42	76.5	0.008	22	41	76.2	0.0080	51	0.95	0.89
2B-1	24706	49	90	67.1	0.006	47	86	65.8	0.0062	277	1.62	0.94
2B-2	19364	40	75	69.6	0.007	39	72	68.6	0.0066	182	1.49	0.89
2B-3	14060	31	58	72.5	0.007	31	57	71.8	0.0071	105	1.43	0.87
2B-4	9302	23	42	76.2	0.008	22	42	75.9	0.0079	52	1.25	0.79
2C-1	26522	52	95	66.6	0.006	49	90	65.2	0.0061	314	1.30	1.03
2C-2	19333	40	75	69.8	0.007	39	72	68.7	0.0066	182	1.20	1.00
2C-3	14056	31	58	72.7	0.007	31	57	72.1	0.0071	105	1.11	0.92
2C-4	9311	23	42	76.2	0.008	22	42	76.0	0.0079	52	1.03	0.85
3C-1	36774	67	109	60.9	0.006	63	101	59.2	0.0057	384	1.36	1.13

3C-2	31245	59	96	62.3	0.006	55	90	60.8	0.0059	288	1.29	1.11
Data set	**Re**	**Nu[(a)]**	**h[(a)]**	**T_{out}[(a)]**	**f[(b)]**	**Nu[(b)]**	**h[(b)]**	**T_{out}[(b)]**	**f**	**ΔP [Pa]**	**TPF**	**TPF_{exp}**
3C-3	26196	51	83	64.0	0.006	49	79	62.7	0.0061	212	1.23	1.05
3C-4	16410	35	58	68.2	0.007	34	56	67.4	0.0068	94	1.11	0.93
4B-1	45715	80	87	49.8	0.005	73	79	48.2	0.0054	172	1.51	1.41
4B-2	30004	57	62	53.1	0.006	53	58	51.7	0.0059	82	1.36	1.25
4B-3	21673	44	48	55.6	0.006	42	46	54.4	0.0064	47	1.28	1.16
4B-4	12566	29	32	59.7	0.007	28	31	59.0	0.0073	18	1.17	1.09
5C-1	39047	70	65	46.9	0.006	65	60	45.3	0.0056	82	1.47	1.47
5C-2	25806	51	47	49.8	0.006	48	44	48.4	0.0061	40	1.32	1.40
5C-3	18640	39	37	51.8	0.007	37	35	50.8	0.0066	22	1.23	1.32
5C-4	10814	25	24	55.8	0.008	25	23	55.2	0.0076	9	1.08	1.25
6B-1	32579	61	47	44.3	0.006	57	43	43.0	0.0058	33	1.57	1.56
6B-2	21134	43	33	46.9	0.006	41	31	45.9	0.0064	16	1.44	1.43
6B-3	15261	33	26	48.9	0.007	32	25	48.0	0.0069	9	1.39	1.38
6B-4	8851	22	17	52.2	0.008	21	16	51.7	0.0080	4	1.39	1.35
7B-1	31946	60	46	45.6	0.006	56	43	44.3	0.0058	33	1.69	1.24
7B-2	21027	43	33	48.2	0.006	41	31	47.1	0.0064	16	1.55	1.19
7B-3	15161	33	26	50.3	0.007	32	25	49.5	0.0069	9	1.50	1.15
7B-4	8758	22	17	54.3	0.008	21	16	53.9	0.0080	4	1.48	1.62
7D-1	32204	60	46	44.5	0.006	56	43	43.1	0.0058	33	1.45	1.09
7D-2	21203	43	33	47.1	0.006	41	32	46.0	0.0064	16	1.30	1.06
7D-3	15190	33	26	49.4	0.007	32	25	48.6	0.0069	9	1.22	1.03
7D-4	8802	22	17	53.1	0.008	21	16	52.6	0.0080	4	1.12	1.03

(a) Nusselt calculated with equation 5.8.
(b) Nusselt calculated with equation 5.9.